Quasi-Phase-Matched Second Harmonic Generation: Tuning and Tolerances

Martin M. Fejer, G. A. Magel, Dieter H. Jundt, and Robert L. Byer, *Fellow, IEEE*

Abstract—**Quasi-phase matching is a technique for phase matching nonlinear optical interactions in which the relative phase is corrected at regular intervals using a structural periodicity built into the nonlinear medium. The theory of quasi-phase-matched second harmonic generation is presented in both the space domain and the wave vector mismatch domain. Departures from ideal quasi-phase matching in periodicity, wavelength, angle of propagation, and temperature are examined to determine the tuning properties and acceptance bandwidths for second harmonic generation in periodic structures. Numerical examples are tabulated for periodically poled lithium niobate. Various types of errors in the periodicity of these structures are then analyzed to find their effects on the conversion efficiency and on the shape of the tuning curve. This analysis is useful for establishing fabrication tolerances for practical quasi-phase-matched devices. A method of designing structures having desired phase-matching tuning curve shapes is also described which makes use of varying domain lengths to establish a varying effective nonlinear coefficient along the interaction length.**

I. Introduction

SOME technique to maintain the relative phase between the interacting waves must be employed to obtain efficient conversion in optical second harmonic generation and other nonlinear optical processes. Quasi-phase matching (QPM) was devised independently by Bloembergen *et al.* [1] and Franken and Ward [2] for this purpose. This invention, which actually predates the development of birefringent phase-matching, corrects the relative phase at regular intervals by means of a structural periodicity built into the nonlinear medium. A particularly effective type of periodic structure is one in which the sign or magnitude of the nonlinear coefficient is modulated throughout the material.

Several experimental demonstrations of quasi-phase-matched optical second harmonic generation (SHG) have been made. It was recognized early that multidomain ferroelectric crystals could show an enhancement of SHG [3]. Rotationally twinned crystals of ZnSe, ZnS, and other materials were considered for the enhancement of SHG by several researchers in the early 1970's [4]–[6]. Levine *et al.* [7] applied a periodic electric field to liquid nitrobenzene to modulate its nonlinear susceptibility for phase matching. Alternating stacks of thin plates of CdTe [8], GaAs [9], [10], quartz [11], and $LiNbO_3$ [11] were constructed by several researchers for QPM SHG experiments. In recent years, $LiNbO_3$ [12], [13] and $LiTaO_3$ crystals [14] and single-crystal fibers [15] having periodically alternating ferroelectric domain structures have been grown for application to QPM SHG. It has also been suggested that QPM may account for the surprisingly high SHG efficiencies sometimes observed in glass fibers [16], [17], and, in fact, periodic electric fields have been intentionally applied to enhance SHG in silica fibers [18].

The results derived in this paper should be useful for analyzing the behavior of practical QPM devices produced by crystal growth, by the stacking of polished plates, by integrated-optic technology in $LiNbO_3$ [19], [20], $LiTaO_3$ [21], KTP [22], or poled nonlinear optical polymer materials [23], or by other field-induced methods. Although we restrict the analysis to second harmonic generation, it can be readily extended to the cases of other nonlinear interactions which can be quasi-phase matched.

We begin with an introduction to the concept of QPM, and derive basic results which will be used in later sections. A region of one sign of the nonlinear coefficient is called a "domain" in analogy with the ferroelectric domains which can be used for this purpose in lithium niobate ($LiNbO_3$). In Section II, perfectly periodic alternating domain structures with planar domain boundaries are assumed, and the acceptance bandwidths for tuning the period, fundamental wavelength, angle of propagation through the structure, and temperature are calculated. Numerical examples are given for periodically poled $LiNbO_3$. Various types of deviations from perfect one-dimensional geometrical periodicity are then analyzed in Section III. The form of phase-matching tuning curves, and a method of designing structures having desired tuning curves, are described in Section IV. Finally, in Section V, periodic phase-matching techniques based on modulation of both the linear and nonlinear susceptibilities are discussed.

A. Quasi-Phase Matching (QPM)

In SHG, a fundamental wave with frequency ω_1 and wavelength λ interacts with the second-order nonlinear susceptibility of a material to produce a polarization wave

Manuscript received April 19, 1991; revised March 9, 1992. This work was supported by the Army Research Office, the Joint Services Eectronics Program, the DARPA Optoelectronic Materials Center, and IBM Corp.

M. M. Fejer, D. H. Jundt, and R. L. Byer are with the Edward L. Ginton Laboratory, Stanford University, Stanford, CA 94305.

G. A. Magel is with Central Research Laboratories, Texas Instruments, Dallas, TX 75265.

IEEE Log Number 9203209.

at the second-harmonic frequency $\omega_2 = 2\omega_1$. Since the polarization wave is forced by the fundamental wave, it travels with the same velocity, determined by n_1, the index of refraction at the fundamental wavelength. The polarization wave radiates a free second-harmonic wave which travels at a velocity determined by n_2, the index of refraction at the harmonic wavelength. In general $n_2 > n_1$ because of normal dispersion in the material, so that the fundamental and second-harmonic waves travel at different phase velocities. Since the sign of power flow from one wave to the other is determined by the relative phase between the waves, the continuous phase slip between these waves caused by their differing phase velocities leads to an alternation in the direction of the flow of power. This situation is illustrated by curve C in Fig. 1(a). It can be seen that the alternation of the sign of power flow leads to a repetitive growth and decay of the second-harmonic intensity along the length of the interaction. The distance over which the relative phase of the two waves changes by π is the "coherence length" $l_c = \lambda/4(n_2 - n_1)$ which is also the half period of the growth and decay cycle of the second harmonic. If the refractive indexes can be matched by some means, for example by using the birefringence of an anisotropic material, the second-harmonic field grows linearly with distance in the medium, and thus the intensity grows quadratically, as shown by curve A. This condition is called "phase matching."

Another method for enabling continuous growth of the harmonic wave along the device, called QPM involves repeated inversion of the relative phase between the forced and free waves after an odd number of coherence lengths. The phase is thus "reset" periodically so that on average, the proper phase relationship is maintained for growth of the second harmonic. One way to invert the phase is to change the sign of the nonlinear coefficient. This can be done, for example, by forming a stack of thin wafers of the nonlinear crystal, rotating alternate wafers by 180°. A more practical approach in ferroelectric crystals like $LiNbO_3$ involves forming regions of periodically reversed spontaneous polarization $\boldsymbol{P}_S$ ("domains"). In materials in which the second-order nonlinearity is induced by an applied electric field, e.g., polymers and liquids, the field can be reversed periodically along the interaction length.

The most rapid growth of the second harmonic, and hence the greatest conversion efficiency, is obtained by changing the sign of $\boldsymbol{P}_S$ (and thus the sign of the nonlinear coefficient) every coherence length. This situation, which we shall call first-order QPM, is illustrated by curve B_1 in Fig. 1(a). Third-order QPM, in which $\boldsymbol{P}_S$ is switched every $3l_c$, is shown by curve B_3 in Fig. 1(b). Note that even-order QPM can also occur when different domain lengths are mixed. For example, second-order QPM can be obtained by using alternating domain lengths of l_c and $3l_c$. In general, mth order QPM entails modulation with period $2ml_c$, where m is an integer.

The above explanation of QPM is a purely "space-domain" description. An alternative view of the effect is obtained by Fourier transformation, so that one examines

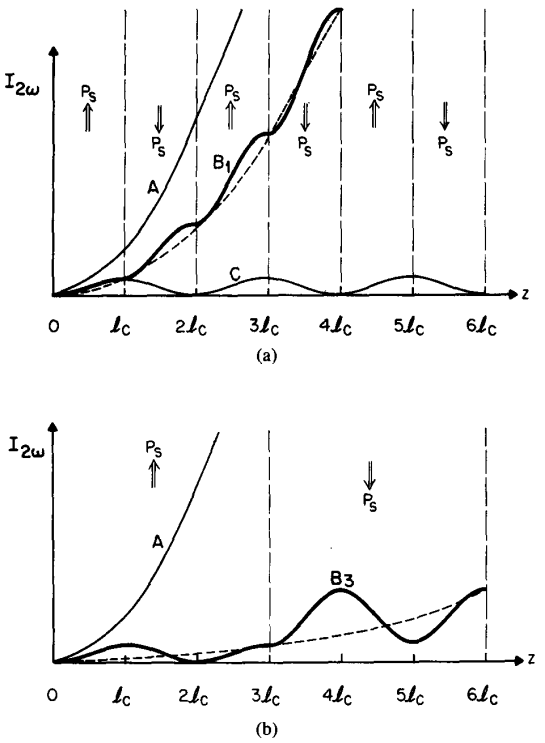

Fig. 1. Effect of phase matching on the growth of second harmonic intensity with distance in a nonlinear crystal. (a) A: perfect phase matching in a uniformly poled crystal; C: nonphase-matched interaction; B_1: first-order QPM by flipping the sign of the spontaneous polarization every coherence length of the interaction of curve C. (b) A: perfect phase matching; B_3: third-order QPM by flipping $\boldsymbol{P}_S$ every three coherence lengths.

the addition of the wave vectors associated with the traveling light waves and with the domain structure, which is a grating in the nonlinear coefficient. This view turns out to be mathematically convenient and often aids the intuition as well. For example, phase-matching occurs when the sum of the wave vectors of the fundamental waves and the nonlinear grating add to equal the wave vector of the second-harmonic wave. It will be easily recognized from the Fourier viewpoint that any periodic structure of the nonlinear coefficient which possesses a spatial harmonic with the proper wave vector can accomplish QPM. Thus, complete sign reversal of the nonlinear coefficient is not required, but simply a modulation of the magnitude of the nonlinear coefficient, with sign reversal being a special (and the most efficient) case.

As can be seen in Fig. 1(a), the second-harmonic power generally grows more slowly even using lowest order QPM than it does with birefringent phase matching. The greatest advantage of QPM lies in its ability to accomplish phase-matching which would otherwise be impossible: in isotropic materials, or in materials which possess in general either too little or too much birefringence at the wavelengths of interest; or using nonlinear coefficients which couple waves of the same polarization. Another important feature is the ability to design a device for operation at

desired wavelengths and temperatures. In addition, the various acceptance bandwidths, as discussed in Section II, can be significantly enhanced for interactions making use of the proper polarizations. The additonal wave vector in the problem makes noncritical phase matching possible in situations where it would not be otherwise, often increasing the angular acceptance bandwidth considerably. Table I lists various bandwidths, along with the coherence lengths and magnitudes of the relevant nonlinear coefficients, for SHG at three different fundamental wavelengths in $LiNbO_3$. Note that structures which accomplish QPM SHG can also be used to phase-match degenerate parametric oscillation or amplification, e.g., the quantities given for SHG with a 2.12 μm fundamental wavelength apply as well to degenerate optical parametric oscillation using a 1.06 μm pump.

It should be noted that phase-matching may also be achieved by modulation of the *linear* susceptibility [26]–[30]. These techniques have been difficult to implement because the amplitude of the linear index modulation must be comparable to the dispersion in order to achieve efficient conversion. The analysis in this paper focuses on structures with modulation of the nonlinear properties. Because the wave vector of the periodic structure required to accomplish QPM is the same for modulation of either the linear or the nonlinear properties, the analysis of Section II and the results in Table I concerning the tuning behavior and phase-matching bandwidths of periodic nonlinear structures should apply equally well to both cases. Other features of "linear" QPM are discussed briefly in Section V, where it is shown that many of the properties of such devices are essentially the same as those for conventional QPM.

TABLE I
FWHM ACCEPTANCE BANDWIDTHS FOR SHG IN CONGRUENT LITHIUM NIOBATE[a]

λ (μm)	Coeff.[b]	l_c (μm)	$\delta\lambda$ (nm)	δT (K)	$\delta\nu^c$ (mrad)	$\delta\nu^d$ (mrad)
0.86	$d_{31(B)}$[e]	—	—	—	—	—
	$d_{31(Q)}$	4.26	0.89	6.0[f]	176	79
	$d_{33(Q)}$	1.67	0.72	13.7[f]	112	103
	$d_{22(Q)}$	1.42	0.60	17.4[f]	104	104
1.064	$d_{31(B)}$[g]	∞	3.18	11.1	∞	102
	$d_{31(Q)}$	129	3.11	9.4	959 (916)	103
	$d_{33(Q)}$	3.40	2.04	25.8	158	146
	$d_{22(Q)}$	2.92	1.74	64	147	147
2.12	$d_{31(B)}$[h]	∞	2317 (303)	9.7	∞	213
	$d_{31(Q)}$	14.4	40	27.5	317	139 (183)
	$d_{33(Q)}$	15.6	62	193 (203)	337	306
	$d_{22(Q)}$	13.4	55	379 (455)	311	311

[a] All values calculated for a 1 mm long crystal using Sellmeier fits from [24] for $T = 25$°C except where noted. Values in parenthesis are from numerical calculations where the linear approximation from (25) is inaccurate.
[b] $d_{31(B)} = d_{31}$, type I, birefringently phase matched; magnitude: 5.9 pm/V
$d_{31(Q)} = 2d_{31}/\pi$, QPM; effective magnitude (d_Q from (23) with $m = 1$): 3.8 pm/V
$d_{33(Q)} = 2d_{33}/\pi$, QPM; effective magnitude: 21.6 pm/V
$d_{22(Q)} = 2d_{22}/\pi$, QPM; effective magnitude: 2.6 pm/V
[c] Rotation around crystallographic z axis; n_e invariant, (41) applies.
[d] Rotation around crystallographic x or y axis; n_e varies with ν, (A1.9) applies.
[e] Birefringent phase matching cannot be achieved at any temperature for this short a wavelength.
[f] Calculated using Sellmeier coefficients from [25] because temperature dependence from [24] cannot be accurately extrapolated to blue wavelengths.
[g] All values on this line calculated at $T_{pm} = -19.4$°C.
[h] All values on this line calculated at $T_{pm} = 580.3$°C.

B. Theoretical Approach

The basic theory of QPM has been discussed by several authors, with emphasis on various nonlinear optical applications [9], [31]–[34] and traveling-wave electrooptic modulators [35]. In addition, extensions of the theory have been made to include the effects of pump depletion [36] and tight focusing [37]. The difficulty in achieving practical QPM devices results from the stringent tolerances placed on the periodic structure, so an analysis of the effects of *departures* from ideal QPM is important. The purpose of this paper is to investigate these effects, which have not been comprehensively discussed in the literature.

In this paper, we analyze SHG as the prototypical second-order nonlinear interaction. We assume low conversion efficiency, loose focusing, CW or long-pulse interaction and no losses for the fundamental or second harmonic waves. Under these conditions, the results for sum or difference frequency generation are essentially the same as those for second harmonic generation, if the appropriate definition of the phase mismatch is used.

The basic slowly varying amplitude equation governing the growth of the second-harmonic field under these conditions is

$$\frac{dE_2}{dz} = \Gamma d(z) \exp(-i\Delta k' z) \tag{1}$$

where E_2 is the amplitude of the second-harmonic field, z is the distance along the propagation direction, $d(z)$ is the spatially varying nonlinear coeffcient for SHG, $\Gamma \equiv i\omega E_1^2/n_2 c$, subscripts 1 and 2 refer to quantities associated with frequencies ω and 2ω, respectively. $\Delta k'$, the wave vector mismatch caused by dispersion in the material, is defined by

$$\Delta k' \equiv k_2 - 2k_1 = \pi/l_c \tag{2}$$

where k_1 and k_2 are the wave vectors at the fundamental and the second harmonic, respectively, and $l_c = \lambda/4(n_2 - n_1)$ is the coherence length. Integrating (1), we find that the second harmonic field at the end of a sample of length L is given by

$$E_2(L) = \Gamma \int_0^L d(z) \exp(-i\Delta k' z)\, dz. \tag{3}$$

For perfect conventional phase matching, i.e., for $d(z) = d_{\text{eff}}$ and $\Delta k' = 0$, the integral in (3) is trivial, and we find that the second harmonic field is given by

$$E_2(L) = \Gamma d_{\text{eff}} L. \tag{4}$$

For QPM interactions, (3) can be analyzed either in terms of the real-space function $d(z)$, or, as may seem natural from the form of the integral, in terms of the Fourier transform of $d(z)$. Consider first the real space description. Assume that $d(z)$ consists of domains of nonlinear coefficient $\pm d_{\text{eff}}$ with sign changes occurring at the positions z_j. Let g_j be the sign and l_j the length of the jth domain. In this case, (3) may be integrated to obtain

$$E_2 = \frac{i\Gamma d_{\text{eff}}}{\Delta k'} \sum_{k=1}^{N} g_k [\exp(-i\Delta k' z_k) - \exp(-i\Delta k' z_{k-1})] \tag{5}$$

where N is the number of domains. The sign changes in a perfect structure occur at positions $z_{k,0}$ which are chosen to satisfy

$$e^{-i\Delta k_0' z_{k,0}} = (-1)^k \tag{6}$$

where $\Delta k_0'$ is the wave vector mismatch at the design wavelength, e.g., for symmetrical odd-order QPM $z_{k,0} = mkl_c$ and for even-order QPM, $z_{k,0} = (mk + (-1)^k) l_c$ [see discussion after (23)]. Phase errors can accumulate due either to deviations of the structure from the prototype or deviations of $\Delta k'$ from the design value. Defining the position error of the kth boundary as $\delta z_k = z_k - z_{k,0}$, and the deviation of the wave vector mismatch from that at the design point as $\delta\Delta k' = \Delta k' - \Delta k_0'$, the accumulated phase error at the kth boundary Φ_k is given by

$$\Phi_k = \Delta k' z_k - \Delta k_0' z_{k,0} \approx \Delta k' \delta z_k + \delta\Delta k' z_{k,0} \tag{7}$$

where the second form neglects a term quadratic in the errors. With (7) we can write (5) for the output field E_2 as

$$E_2 = \frac{i\Gamma g_1 d_{\text{eff}}}{\Delta k'} \left[2 \sum_{k=1}^{N-1} e^{-i\Phi_k} + (e^{-i\Phi_N} + 1) \right]. \tag{8}$$

As the contribution of the final two terms of (8) is smaller than that of a single period, in most cases of interest, i.e., for $N >> 1$, we can approximate (8) as [36],

$$E_2 = \frac{i2\Gamma g_0 d_{\text{eff}}}{\Delta k'} \sum_{k=1}^{N} e^{-i\Phi_k} \tag{9}$$

which we use extensively in Section III. For a perfect structure, i.e., one with $\Phi_j = 0$ for $1 < j < N$, the sum in (9) is just N. Noting that for a perfect structure $N = L/ml_c = L\Delta k'/m\pi$, (9) becomes

$$E_{2,\text{ideal}} \approx i\Gamma g_1 d_{\text{eff}} \frac{2}{m\pi} L. \tag{10}$$

Comparing (4) and (10), we see that in an interaction with perfect mth order QPM, the effective nonlinearity is reduced by a factor of $2/m\pi$ compared to that of a conventionally phase-matched interaction.

Another approximate form convenient for computation can be obtained by noting the similarity, for symmetrical odd-order QPM, of the quantity in square brackets in (8) to the trapezoidal rule approximation to the integral of a continuous function $\Phi(z)$ chosen such that

$$\Phi(z_{k,0}) = \Phi_k \tag{11}$$

i.e. by noting that

$$\sum_{k=1}^{N-1} e^{-i\Phi_k} + \frac{1}{2}(e^{-i\Phi_N} + 1) \approx \frac{1}{ml_c} \int_0^L e^{-i\Phi(z)}\, dz. \tag{12}$$

The error in this approximation, which can be shown with the usual analysis applied to numerical quadrature to typically scale as Φ/N^2, is negligible in many practical situations. Combining (12) with (8) and (10), we have

$$E_2/E_{2,\text{ideal}} \approx \frac{1}{L} \int_0^L e^{-i\Phi(z)}\, dz. \tag{13}$$

This integral form is particularly convenient for the calculation of tuning curves, as seen in Section IV. Equation (13) can similarly be shown to apply for nonsymmetric odd- and even-order QPM.

Now consider the Fourier transform approach. Let us write the normalized form of $d(z)$ as

$$g(z) \equiv d(z)/d_{\text{eff}} \tag{14}$$

and generalize the previous calculation by allowing $g(z)$ to take any value between -1 and 1 for $0 < z < L$. Equation (3) than takes the form

$$E_2 = \Gamma d_{\text{eff}} L G(\Delta k') \tag{15}$$

where $G(\Delta k')$, the transform of $g(z)$, is given by

$$G(\Delta k') = \frac{1}{L} \int_0^L g(z) \exp(-i\Delta k' z)\, dz. \tag{16}$$

Since G is a function of $\Delta k'$, we refer to the transform domain as the "mismatch domain," and $G(\Delta k')$ as the "mismatch function." [38] Comparing (4) and (15), we see that the magnitude of the mismatch function, which is less than or equal to 1, represents the reduction in the effective nonlinearity compared to a conventionally phase-matched medium. Since the squared magnitude of the mismatch function is proportional to the conversion efficiency, it is, up to a scale factor in the abscissa, the same as the tuning curve obtained by varying $\Delta k'$ with temperature, wavelength, etc.

If $g(z)$ is a function periodic in z with period Λ, i.e.,

$$g(z) = \sum_{m=-\infty}^{\infty} G_m e^{iK_m z} \tag{17}$$

whose mth-harmonic grating wave vector

$$K_m = \frac{2\pi m}{\Lambda} \tag{18}$$

is close to $\Delta k'$, the integral in (16) is dominated by the contribution of this mth term, and (15) thus can be written

$$E_2 \approx ie^{-\Delta kL/2} \Gamma d_Q L \operatorname{sinc}(\Delta kL/2) \tag{19}$$

where $d_Q = d_{\text{eff}} G_m$ is the amplitude of the relevant harmonic of $d(z)$,

$$\Delta k \equiv k_2 - 2k_1 - K_m \tag{20}$$

is the total wave vector mismatch, and sinc $(x) \equiv \sin(x)/x$. The behavior of the QPM interaction is similar to that of a conventionally phase-matched interaction, but with an effective mismatch Δk shifted by an amount K_m with respect to $\Delta k'$, and an effective nonlinear coefficient d_Q in place of d_{eff}.

As an example of the utility of thinking in the mismatch domain, we determine the effect of duty cycle on the conversion efficiency. Let $g(z)$ be a rectangular wave of period Λ taking the values ± 1, with the positive sections of length l. The duty cycle is defined by

$$D \equiv l/\Lambda. \tag{21}$$

Assuming that the $+m$ term of the complex Fourier series for $g(z)$ is phase matched, i.e., assuming $K_m = \Delta k'$, the corresponding Fourier coefficient is found using a standard transform pair to be

$$G_m = \frac{2}{\pi m} \sin(\pi m D). \tag{22}$$

Since $d_Q = d_{\text{eff}} G_m$, we find that at optimum D, for which the sine factor is unity,

$$d_Q = \frac{2 d_{\text{eff}}}{\pi m} \tag{23}$$

in agreement with the real space result in (10). The conversion efficiency, proportional to d_Q^2, is thus reduced by $(2/\pi m)^2$ compared to a conventionally phase-matched interaction. Equation (22) also shows that the optimum duty cycle for odd m is 50%. (Actually, as m grows larger, there is more than one optimum duty cycle which makes the sine term equal to 1.) The fact that the optimum D for $m = 2$ is 25% or 75% agrees with the result stated earlier that second-order QPM corresponds to alternating domains of l_c and $3l_c$.

II. Tuning and Bandwidths in Periodic Structures

To evaluate the utility of quasi-phase-matched devices for practical applications, it is important to establish tolerances for variations in temperature, wavelength, etc. by evaluating their effects on the efficiency of the device. For a device of total length L containing uniform periods, the phase-matching factor in the expression for the power conversion efficiency is, according to (19), $\text{sinc}^2(\Delta k L/2)$, so that the QPM peak has the same shape as that of conventionally phase-matched device, but has been shifted by the wave vector of the periodic structure away from the bulk value of $\Delta k'$. We may use the fact that this factor goes to $1/2$ when $\Delta k L/2 = 0.4429\pi$ to find the full width at half maximum (FWHM) acceptance bandwidths for several quantities which affect Δk when they are varied. It is also of interest to calculate how rapidly the phase-matched wavelength tunes with variations in the parameter ζ.

In general, Δk as a function of a parameter ζ and the wavelength λ may be expanded in a Taylor series about the value ζ_0 which achieves QPM for $\lambda = \lambda_0$ (so that $\Delta k(\zeta_0, \lambda_0) = 0$):

$$\Delta k(\zeta, \lambda) = (\zeta - \zeta_0) \frac{\partial \Delta k}{\partial \zeta} + (\lambda - \lambda_0) \frac{\partial \Delta k'}{\partial \lambda} + \frac{1}{2} (\zeta - \zeta_0)^2 \frac{\partial^2 \Delta k}{\partial \zeta^2} + \cdots. \tag{24}$$

Note that the form of the second term in (24) explicitly takes into account that K is independent of λ. If Δk has a first-order dependence on ζ, then we usually may neglect the higher-order terms in the expansion. The FWHM bandwidth in ζ, which we will denote by $\delta\zeta$, is found by fixing $\lambda = \lambda_0$ and solving (24) for the value of $(\zeta - \zeta_0)$ which satisfies $\Delta k L/2 = 0.4429\pi$ and then doubling it. This procedure gives

$$\delta\zeta = \frac{5.57}{L} \left| \frac{\partial \Delta k}{\partial \zeta} \right|^{-1}. \tag{25}$$

We will use this result throughout this section to calculate bandwidths for period, fundamental wavelength, angle of incidence, and temperature. The rate at which the phase-matched wavelength tunes with ζ can be obtained by setting (24) equal to zero and solving for $(\lambda - \lambda_0)$ in terms of $(\zeta - \zeta_0)$. We find

$$\lambda - \lambda_0 = \frac{\partial \Delta k/\partial \zeta}{\partial \Delta k'/\partial \lambda} (\zeta - \zeta_0) = \frac{\delta\lambda}{\delta\zeta} (\zeta - \zeta_0) \tag{26}$$

where the second form follows from the first and (25).

The analysis in this section is directed to collinear or nearly collinear interactions. Interaction between counterpropagating beams, which are possible in QPM devices, are discussed briefly in Appendix III.

A. Constant Period Error

Let the domain structure be perfectly periodic but with the wrong period $\Lambda \approx 2ml_c$, near that required for mth-order QPM. Writing (20) as

$$\Delta k = \Delta k' - \frac{2\pi m}{\Lambda} \tag{27}$$

we obtain

$$\frac{\partial \Delta k}{\partial \Lambda} = \frac{2\pi m}{\Lambda^2} = \frac{\pi}{2ml_c^2}. \tag{28}$$

Thus, the FWHM acceptance width for the period is, according to (25) and (28),

$$\delta\Lambda = \frac{3.55 m l_c^2}{L} = \frac{1.77\Lambda}{Nm} \tag{29}$$

where $N = L/ml_c$ is the number of domains in the sample. When the conversion efficiency has dropped to half, i.e., when the error in period is $\delta\Lambda/2$, the accumulated error in the position of the Nth domain boundary is $N\delta\Lambda/4 = 0.886l_c$, independent of the order of the QPM.

B. Spectral Bandwidth

Since tuning the fundamental wavelength λ has no effect on the periodicity of the structure, the only contribution to the derivation of Δk comes from the material term $\Delta k'$. The result for the spectral bandwidth, obtained from (18) and (24) with $\zeta = \lambda$, is

$$\delta\lambda = \frac{0.4429\lambda}{L}\left|\frac{n_2 - n_1}{\lambda} + \frac{\partial n_1}{\partial\lambda} - \frac{1}{2}\frac{\partial n_2}{\partial\lambda}\right|^{-1} \quad (30)$$

where the derivatives are evaluated at their respective wavelengths. Note that the term $(n_2 - n_1)/\lambda$ in (30) for QPM vanishes in the similar expression for conventional phase matching, because $n_2 = n_1$ in the latter case.

The indexes and dispersion can be obtained numerically, for example, from published Sellmeier fits for the material being used. Table I contains a column comparing spectral bandwidths for SHG in $LiNbO_3$ for various polarizations and wavelengths. At longer wavelengths the bandwidths tend to increase because of the decrease in dispersion.

C. Angle Tuning and Angular Acceptance

The QPM condition depends on the angle between the grating vector $\boldsymbol{K}$ and the fundamental wave vector $\boldsymbol{k}_1$. The implications of this effect are similar to those of the angular dependence of the extraordinary index of refraction in a birefringently phase-matched device. It is both a means for tuning the phase-matching condition and a limitation on the angular acceptance bandwidth. As QPM is often carried out in birefringent crystals, both QPM effects and birefringence effects can occur simultaneously. We will first analyze QPM in an isotropic medium to uncover those effects due purely to QPM, and then briefly discuss the modifications necessary for QPM in anistropic crystals.

Consider first the phase-matched case, with the geometry indicated in the wave vector diagram of Fig. 2(a). The angle within the sample between the fundamental wave vector $\boldsymbol{k}_1$ and the periodic structure wave vector $\boldsymbol{K}$ is θ, where for notational convenience we use $\boldsymbol{K}$ rather than $\boldsymbol{K}_m$ to indicate the spatial harmonic contributing to the QPM. The angle ψ between $\boldsymbol{k}_1$ and the wave vector of the forced second harmonic wave, and hence the angle between $\boldsymbol{k}_1$ and the QPM free second harmonic wave, can be calculated from Fig. 2(a) and the law of sines. We find

$$\sin\psi = \frac{K}{k_2}\sin\theta \quad (31)$$

so that if $\theta \neq 0$, then $\psi \neq 0$ and the phase velocity of the second harmonic output will not be parallel to the fundamental input. While the effects of this "walkoff" on the efficiency of the interaction are similar to those of a walkoff in a conventional birefringently phase-matched interaction, it is important to note that in the case of QPM the walkoff is related to the phase velocities of the interacting waves (wave vectors) and can occur in isotropic media, while the walkoff in the conventional case is related to the group velocity (Poynting vectors) and occurs only in anisotropic media. In either case, the walkoff reduces the efficiency by limiting the interaction length to the "aperture length" $l_a = \pi^{1/2}w_1/\psi$, where w_1 is the Gaussian beam waist of the fundamental [39]. We have to this point considered only the positive spatial frequency component of the grating $\boldsymbol{K}$ and neglected the negative frequency component $-\boldsymbol{K}$. In general this neglect is justified because $-\boldsymbol{K}$ will be far from phase matching. In the special case where $\theta = 90°$, QPM will be possible using both $\boldsymbol{K}$ and $-\boldsymbol{K}$, resulting in two second harmonic beams emerging at $\pm\psi$.

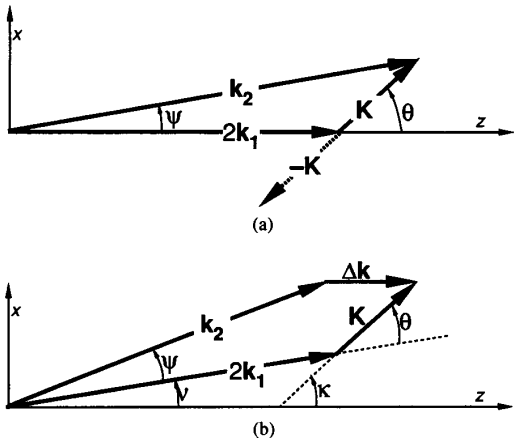

Fig. 2. Wave vector diagram for QPM angle tuning analysis. (a) Phase-matched case. (b) Nonphase-matched case.

For a given fundamental wavelength λ, the period required for mth order QPM at an angle θ can be found using the law of cosines to be

$$\Lambda = \frac{m\lambda}{2n_2}\left[\sqrt{1 - \left(\frac{n_1}{n_2}\sin\theta\right)^2} - \frac{n_1}{n_2}\cos\theta\right]^{-1}. \quad (32)$$

For $\theta = 0$, (32) reduces to $\Lambda = \Lambda_0$, where, in agreement with our previous results,

$$\Lambda_0 = \frac{m\lambda}{2(n_2 - n_1)}. \quad (33)$$

Equation (32) is well approximated by a parabola up to angles as large as ~ 0.4 rad. This simpler form is

$$\Lambda \approx \Lambda_0\left(1 - \frac{1}{2}\frac{n_1}{n_2}\theta^2\right). \quad (34)$$

A somewhat more accurate expression can be obtained by expanding (32) to first order in $n_2 - n_1$,

$$\Lambda \approx \Lambda_0 \cos\theta\left(1 + \frac{n_2 - n_1}{2n_2}\tan^2\theta\right). \tag{35}$$

For values of n_1/n_2 corresponding to SHG of visible wavelengths in $LiNbO_3$, we find that (35) is accurate to within 1% of the exact value obtained using (32) for θ as large as 1 rad.

To determine the dependence of the phase-matching wavelength on the angle θ, we evaluate the condition $2ml_c(\lambda) = \Lambda_{\text{eff}}(\theta)$ to lowest nonvanishing order. Near $\theta = 0$, we find with (34) that

$$\lambda_{\text{pm}}(\theta) \approx \lambda_0 + \frac{n_1}{2n_2} l_c(\lambda_0)\left[\frac{\partial l_c}{\partial\lambda}\bigg|_{\lambda_0}\right]^{-1}\theta^2 \tag{36}$$

where λ_0 is the wavelength which quasi-phase matches when $\theta = 0$. A similar expression can be obtained for the phase-matching temperature as a function of angle.

We now address the question of angular acceptance bandwidths due to the periodic domain structure. We assume that the refractive index is isotropic, or at least that the wave vector surfaces are of circular cross-section in the plane in which the sample is tilted. This condition holds, for example, for both refractive indexes if propagation is in the plane perpendicular to the optic axis in a uniaxial crystal, or for propagation in any plane if the interaction involves only ordinary waves. The geometry considered is shown in Fig. 2(b). The fundamental radiation propagates with wave vector $\boldsymbol{k}_1$ in the $x - z$ plane at an angle ν to the normal (z) to the surface of the crystal. The grating wave vector lies at an angle θ to $\boldsymbol{k}_1$, and at an angle κ to z. The free second harmonic wave propagates with wave vector $\boldsymbol{k}_2$ at an angle ψ to $\boldsymbol{k}_1$.

For $\theta \neq 0$ the situation is analogous to critical phase matching, and, according to (25) we need the derivative $\partial\Delta k/\partial\nu$ to evaluate the angular acceptance bandwidth. With the assumed geometry, the boundary conditions for the second harmonic require

$$k_{2x} = 2k_{1x} + K_x \tag{37}$$

and from geometry we have $\Delta\boldsymbol{k} = \Delta k\hat{z}$, where

$$\Delta k = k_{2z} - 2k_{1z} - K_z \tag{38}$$

and subscripts x and z indicate Cartesian components of vectors.

We find from (37) and (38) that the required derivative is

$$\frac{\partial\Delta k}{\partial\nu} = -2k_1 \sin\psi/\cos(\nu + \psi). \tag{39}$$

Evaluating (39) for the phase-matched case and using the result in (25), we find for the FWHM angular bandwidth

$$\begin{aligned}\delta\nu &= \frac{5.57}{L}\left|\frac{\partial\Delta k}{\partial\nu}\right|^{-1}_{\nu=\nu_{PM}} \\ &= \frac{5.57\cos\nu}{KL\sin(\kappa - \nu)}\left[1 + \frac{\cos\kappa}{\cos\nu}\frac{K}{2k_1}\right] \qquad (\theta \neq 0) \\ &\approx 0.886\frac{\cos\nu}{\sin(\kappa - \nu)}\frac{\Lambda}{L}\end{aligned} \tag{40}$$

where the approximate form follows by assuming $K \ll 2k_1$. From (40) we see that for critical phase-matching the angular bandwidth is inversely proportional to the length of the device, and, noting that $\Lambda/L = 2/N$, inversely proportional to the number of domains.

Near $\theta = 0$, Δk has no first order dependence on ν, the QPM is noncritical, and the bandwidth is determined by the second order term in (24). Taking the derivative of (39) with respect to ν, and using the resulting second derivative in a Taylor series expansion of Δk in ν, we obtain the FWHM angular acceptance for a noncritically phase-matched interaction

$$\delta\nu = 2\sqrt{1.772\frac{n_2}{n_1}\frac{l_c}{L}\cos\nu} \qquad (\theta = 0). \tag{41}$$

We see that the bandwidth for this case depends inversely on the square root of the device length, which results in a greatly enhanced bandwidth compared to critical phase-matching for samples containing many periods. Some angular acceptance bandwidths for noncritical QPM are tabulated in Table I.

These results may be readily generalized to the anisotropic case, in which the wave vector surfaces are noncircular in cross section, as briefly discussed in Appendix I. The essential difference between QPM in isotropic and in anisotropic media is that in the latter at least one of the indexes of refraction depends on ν. This dependence has a straightforward effect on the angle tuning rate, and also leads to Poynting vector walkoff for wave vectors not parallel to an optical axis. It is possible to eliminate walkoff (have parallel group velocities) for a structure with $\theta \neq 0$ (which has an angle ψ between $\boldsymbol{k}_2$ and $\boldsymbol{k}_1$) by using a propagation direction chosen such that the Poynting vector walkoff is equal and opposite to the phase velocity walkoff. A similar effect has been observed in conventionally phase-matched devices using noncollinear angle phase-matching for parametric interactions [40], [41]. It is clear that the results in this section apply equally well to angle tuning in planar waveguides, but must be modified for channel devices. In this case, defining θ as the angle between $\boldsymbol{K}$ and the waveguide axis, (35) is replaced by $\Lambda = \Lambda_0\cos(\theta)$ from which it follows that (36) with $n_1 = n_2$ correctly describes channel waveguide QPM. Note that while Poynting vector walkoff does not occur in this configuration, the transverse phase variation due to K_x must be incorporated into the overlap integral for the waveguide interaction.

D. Temperature Bandwidth

When the temperature is tuned, in addition to the change in $\Delta k'$ caused by the temperature dependence of the refractive indexes, thermal expansion can alter both the period Λ and the total length L of the device. We must therefore take the derivative with respect to temperature of the product ΛkL instead of Δk alone. Since $\Delta k = \Delta k' - K$, we have

$$\frac{\partial}{\partial T}(\Delta kL) = L\left(\frac{\partial \Delta k'}{\partial T} - \frac{\partial K}{\partial T}\right) + (\Delta k' - K)\frac{\partial L}{\partial T}. \quad (42)$$

With the coefficient of linear thermal expansion α defined as $\alpha = l^{-1}\,\partial l/\partial T$, we have $\partial L/\partial T = \alpha L$ and $\partial K/\partial T = -\alpha K$, so the terms involving K in (42) cancel, leaving

$$\frac{\partial}{\partial T}(\Delta kL) = L\frac{\partial \Delta k'}{\partial T} + \alpha \Delta k' L = \frac{\pi L}{l_c}\left[\frac{1}{\Delta n}\frac{\partial \Delta n}{\partial T} + \alpha\right] \quad (43)$$

where $\Delta n = n_2 - n_1$. Note that (43) is independent of the period of the domain structure.

To calculate the temperature acceptance bandwidth, we insert (43) into (25) to obtain

$$\delta T = \frac{0.4429\lambda}{L}\left|\frac{\partial \Delta n}{\partial T} + \alpha \Delta n\right|^{-1} \quad (44)$$

where, as before, $\Delta n \equiv n_2 - n_1$. As was noted for the spectral bandwidth, the fact that QPM allows the use of the same polarization for both the fundamental and second harmonic can lead to a substantial increase in bandwidth, particularly if a refractive index is used whose dispersion is relatively temperature insensitive. See Table I again for a comparison of temperature bandwidths for SHG in $LiNbO_3$. Like the spectral bandwidths, thermal bandwidths increase toward longer wavelengths.

III. Quasi-Phase Matching in Nonideal Structures

In this section deviations from regularity in quasi-phase-matching structures which tend to reduce the efficiency are addressed. Variations in domain length along the direction of propagation (which we refer to as longitudinal variations) cause phase errors which disturb the phase matching. For the following analyses, we assume that only complete sign reversal of the nonlinear coefficient is possible. Thus for longitudinal variations, the domain reversal pattern $g(z)$ of (6) takes the form of a rectangular wave with a locally well-defined, if not constant, duty cycle and period.

Qualitative understanding of the effects of deviations from periodicity in the QPM structure can be obtained from the Fourier or "mismatch domain" analysis discussed in Section I-B, according to which the second harmonic output field is proportional to the component of the domain reversal pattern $g(z)$ at the spatial frequency $\Delta k'$. For an ideal structure of length L the FWHM of the transform $G(z)$ is approximately $2\pi/L$, so that deviations in the domain reversal that cause a comparable or larger shift or broadening of the transform will lead to significant reductions in the conversion efficiency.

Quantitative analysis of these effects for particular types of errors can be carried out in either domain. In the remainder of this section we use a real space description. Results for the second harmonic field E_2 and conversion efficiency η including the effects of various errors are normalized to the field $E_{2\,\text{ideal}}$, and the conversion efficiency η_{ideal} expected for an ideal QPM structure of the same order m. From (10) we have

$$E_{2,\text{ideal}} = i\Gamma g_0 2d_{\text{eff}} L/m\pi \quad (45)$$

and

$$\eta_{\text{ideal}} = \left|\frac{E_{2,\text{ideal}}}{E_1}\right|^2 = \left|\frac{2\omega d_{\text{eff}} E_1 L}{\pi n_2 cm}\right|. \quad (46)$$

Thus, according to (9),

$$\hat{E}_2 \equiv E_2/E_{2,\text{ideal}} = \frac{1}{N}\sum_{k=1}^{N} e^{-i\Phi_k} \quad (47)$$

and

$$\hat{\eta} \equiv I_2/I_{2,\text{ideal}} = \frac{1}{N^2}\left|\sum_{k=1}^{N} e^{-i\Phi_k}\right|^2 \quad (48)$$

where I_2 is the second harmonic output intensity and Φ_k was defined in (7) as the phase error at the kth boundary,

$$\Phi_k = \Delta k'\delta z_k + \delta \Delta k' z_{k,0}. \quad (7)$$

A. Missing Reversals

Flaws in a lithographically defined periodic structure or fluctuations during the growth of bulk periodic crystals can lead to missing domains. Assuming that the structure is not otherwise disturbed, each such missing reversal combines three of the ideal domains into one domain an odd number of coherence lengths long, thereby reducing the total number of domains by 2.

According to (9), we can write

$$\hat{E}_2 = \frac{1}{N}\sum_{k=1}^{N'} e^{-i\Phi_k} \quad (49)$$

where N' is the number of domains in the perturbed device. According to the previous discussion, if there are M missing domains, $N' = N - 2M$. Since all the domains are an odd number of coherence lengths long, no matter what the distribution of the M missing domains, all the Φ_k obey $\Phi_k = 2p_k\kappa$, where p_k is an integer or zero, so (49) can be written

$$\hat{E}_2 = \frac{N - 2M}{N} = 1 - 2f \quad (50)$$

where $f = M/N$ is the fraction of domains with sign opposite that of the ideal prototype structure. Since (50) is based on the approximate (9), it neglects a contribution

to E_2 on the order of that of one domain. Note that $f = 1/2$ represents a single domain structure, for which E_2 vanishes to this level of approximation, while $f = 1$ represents a perfect structure with each domain of sign opposite that of the prototype, for which the magnitude of E_2 is unchanged, but the sign is reversed. From (46) and (50) we have

$$\hat{\eta}_{\text{miss rev}} = (1 - 2f)^2. \tag{51}$$

B. Random Errors in Positions of Domain Boundaries

We now consider a structure which has the same number of domains as the prototype, but also has random errors in the length of the domains. Since we have only statistical information about the positions of the boundaries of the domains, we can calculate only expected values of the various quantities of interest. Before introducing the statistical description of the boundary positions, it is useful to manipulate the expression for the normalized efficiency given in (48) into a form more convenient for statistical analysis. We begin by expressing the squared magnitude as a double sum

$$\hat{\eta} = \frac{1}{N^2} \sum_{k=1}^{N} \sum_{j=1}^{N} e^{-i(\Phi_k - \Phi_j)}. \tag{52}$$

The N terms with $j = k$ are all equal to 1, so we can separate these terms and sum them explicitly, yielding

$$\hat{\eta} = \frac{1}{N} + \frac{1}{N^2} \sum_{k=1}^{N} \sum_{j \neq k}^{N} e^{-i(\Phi_k - \Phi_j)} \tag{53}$$

Dividing the inner sum into two parts with $j < k$ and $j > k$, and reversing the order of summation for the latter, yields

$$\hat{\eta} = \frac{1}{N} + \frac{1}{N^2} \sum_{k=1}^{N-1} \sum_{j=k+1}^{N} [e^{-i(\Phi_k - \Phi_j)} + e^{-i(\Phi_j - \Phi_k)}]. \tag{54}$$

Reindexing the inner sum with $p = j - k$, we have

$$\hat{\eta} = \frac{1}{N} + \frac{2}{N^2} \sum_{k=1}^{N-1} \sum_{p=1}^{N-k} \cos(\Phi_k - \Phi_{k+p}). \tag{55}$$

If only statistical information is available for the phase errors, we can calculate only ensemble averages of the efficiency. With (55) we obtain

$$\begin{aligned} \langle \hat{\eta} \rangle &= \frac{1}{N} + \frac{2}{N^2} \sum_{k=1}^{N-1} \sum_{p=1}^{N-k} \langle \cos(\Phi_k - \Phi_{k+p}) \rangle \\ &= \frac{1}{N} + \frac{2}{N^2} \sum_{k=1}^{N-1} \sum_{p=1}^{N-k} \langle \cos(\Delta\Phi_{k,p}) \rangle \end{aligned} \tag{56}$$

where the angle brackets indicte an ensemble average, and in the second line we use the notation $\Delta\Phi_{k,p} = \Phi_{k,p} - \Phi_k$ for the phase error accumulated between layers k and $k + p$. If the phase errors vanish, the summand is 1, the inner sum is trivial, the outer sum is an arithmetic series, and the normalized efficiency can be shown to equal unity. In the presence of large random phase errors, the sum vanishes, and the normalized efficiency approaches $1/N$, as would be expected for the incoherent sum of the contributions of N layers.

To make further progress, we need to specify the errors δz_k in the positions of the domain boundaries. At least two types of randomly perturbed structures are of interest. If a collection of plates of varying thickness are stacked to form the structure, the error in the position of the kth boundary is the sum of the errors in the thickness of the all the previous layers, so that the errors grow with k in the manner of a random walk. We refer to this type of structure as having a random period error. If instead the domains are fabricated by a method, e.g., lithography, that maintains the average position of the boundaries with uniform accuracy across the whole device, but local effects randomly perturb the position of each boundary, the probable error in the kth boundary is independent of k. We refer to this type of structure as having a random duty cycle error.

In both these cases, it is useful to describe the distribution of domain boundaries in terms of a more readily observed quantity, the lengths of the domains, where the lengths l_k are given by

$$l_k = z_k - z_{k-1} \tag{57}$$

so that the errors in the domain lengths δl_k are given by

$$\delta l_k = \delta z_k - \delta z_{k-1}. \tag{58}$$

Consider first random duty cycle errors. If we assume that errors in the positions of the boundaries have zero mean, it is clear from (58) that $\langle \delta l_k \rangle = 0$, and, from the assumption that the errors in boundary position are independent and stationary with respect to k, that the variances are related by

$$\sigma_l^2 = 2\sigma_z^2 \tag{59}$$

where the now irrelevant k subscript has been suppressed.

In the case of random period errors, it is useful to rewrite (57) as

$$z_k = \sum_{j=1}^{k} l_j \tag{60}$$

and hence that

$$\delta z_k = \sum_{j=1}^{k} \delta l_j. \tag{61}$$

Assuming that the δl_k are distributed with zero mean and are indepenent and stationary with respect to k, we have $\langle \delta z_k \rangle = 0$, and from (61)

$$\sigma_{z_k}^2 = k\sigma_l^2. \tag{62}$$

Note that even though the l_k are identically distributed, the z_k are not.

With (57)–(62) and (7), we can obtain the mean and variance of $\Delta\Phi_{k,p}$, necessary for the evaluation of (56).

We find

$$\langle \Delta\Phi_{k,p} \rangle = \delta\Delta k' \langle z_{k+p,0} - z_{k,0} \rangle = \delta\Delta k' p m l_c$$

$$\sigma^2_{\Delta\Phi_{k,p}} = \begin{cases} (\Delta k_0')^2 2\sigma_z^2 = (\Delta k_0')^2 \sigma_l^2 \\ \quad \text{duty cycle errors} \\ (\Delta k_0')^2 (\sigma^2_{zk,p} - \sigma^2_{zk}) = (\Delta k_0')^2 p \sigma_l^2 \\ \quad \text{period errors.} \end{cases} \tag{63}$$

Note that both the mean and the variance of $\Delta\Phi_{k,p}$ given in (63) are independent of the position k, depending only on the separation of the layers p as might be expected from the stationary forms assumed for the errors. This behavior can be made explicit using a simpler notation dropping the subscript k, i.e., $\langle \Delta\Phi_{k,p} \rangle \rightarrow \langle \Delta\Phi_p \rangle$ and $\sigma^2_{\Delta\Phi_{k,p}} \rightarrow \sigma^2_{\Delta\Phi_p}$.

In addition to specifying the mean and the variance of the errors, it is necessary to specify their distribution function. In general this function is not known *a priori*, so we assume that the errors are normally distributed, which both leads to simple mathematical results and has some justification from the central limit theorem as a description for the sum of independent errors. The probability density function for the phase error accumulated between layers k and $k + p$ then takes the form

$$p_{\Delta\Phi}(\Delta\Phi_{k,p}) = \frac{1}{\sqrt{2\pi}\ \sigma_{\Delta\Phi_p}} \exp\left(- \frac{(\Delta\Phi_{k,p} - \langle \Delta\Phi_p \rangle)^2}{2\sigma^2_{\Delta\Phi_p}} \right). \tag{64}$$

With this probability density function, we can evaluate the mean value appearing in the summand of (55):

$$\begin{aligned} \langle \cos(\Delta\Phi_{k+p}) \rangle &= \int_{-\infty}^{\infty} p_{\Delta\Phi}(\Delta\Phi_{k+p}) \cos(\Delta\Phi_{k+p})\, d\Delta\Phi_{k+p} \\ &= \frac{1}{\sqrt{2\pi}\ \sigma_{\Delta\Phi_p}} \int_{-\infty}^{\infty} \\ &\quad \cdot \exp\left(- \frac{[\Delta\Phi_{k+p} - \langle \Delta\Phi_p \rangle]^2}{2\sigma^2_{\Delta\Phi_p}} \right) \\ &\quad \cdot \cos(\Delta\Phi_{k+p})\, d\Delta\Phi_{k+p} \\ &= e^{-\sigma^2_{\Delta\Phi_p}/2} \cos(\langle \Delta\Phi_p \rangle) \end{aligned} \tag{65}$$

where the first equality follows from the definition of the mean value, the second from (63) and (64), and the last from a standard definite integral.

We now have the information necessary to calculate the efficiency in the presence of random errors by evaluating the sum in (55). Assume that the device is tuned to the nominal operating point, so that $\delta\Delta k' = 0$. Consider first the case of random duty cycle errors. According to (63), the variance of the phase error is independent of p and is given by

$$\sigma^2_{\Delta\Phi_p} = \pi^2 \sigma_l^2 / l_c^2 = \sigma_\phi^2 \tag{66}$$

where σ_ϕ^2 is defined implicitly in (66). Noting that according to (65) and (66) the summand in (55) is independent of p and k, the summation is trivial and we find

$$\langle \hat{\eta} \rangle = e^{-\sigma_\phi^2/2} + \frac{1}{N}(1 - e^{-\sigma_\phi^2/2}). \tag{67}$$

For a perfect structure ($\sigma_\phi \rightarrow 0$), the normalized efficiency goes to 1 as it should. For large errors, the normalized efficiency approaches $1/N$, as is appropriate for the incoherent sum of the output of N layers. For large N and moderate errors, the second term in (67) is negligible, the normalized efficiency is a function only of σ_ϕ, and we have

$$\begin{aligned} \langle \hat{\eta} \rangle &\approx e^{-\sigma_\phi^2/2} \\ &\approx 1 - \pi^2 \sigma_l^2 / (2 l_c^2) \end{aligned} \tag{68}$$

where the second approximation follows from (67) and an expansion to lowest order in σ_l. The tolerance on the rms error for $>50\%$ conversion is obtained from (68) as

$$\sigma_l / l_c < \sqrt{2 \ln 2}/\pi = 0.375. \tag{69}$$

We see that the sensitivity to duty cycle errors is rather small, with rms errors as large as one third of a coherence length reducing the efficiency by less than 50%.

Now consider the case of random period errors. The random walk accumulation of phase error both leads to substantially greater degradation of the efficiency, and complicates the analysis. We may still use (65) to evaluate $\langle \cos(\Delta\Phi_{k+p}) \rangle$, but using (63) for $\sigma^2_{\Delta\Phi_p}$ we obtain

$$\sigma^2_{\Delta\Phi_p} = p\pi^2 \sigma_l^2 / l_c^2 = p\sigma_\phi^2 \tag{70}$$

where σ_ϕ, implicitly defined in (66), is independent of p. With (65) and (70), (55) takes the form

$$\langle \hat{\eta} \rangle = \frac{1}{N} + \frac{2}{N^2} \sum_{k=1}^{N-1} \sum_{p=1}^{N-k} e^{-p\sigma_\phi^2/2}. \tag{71}$$

The p dependence of the summand complicates the summation. Noting that the inner sum is a geometric series, we have

$$\begin{aligned} \langle \hat{\eta} \rangle &= \frac{1}{N} + \frac{2}{N^2} \frac{1}{e^{\sigma_\phi^2/2} - 1} \sum_{k=1}^{N-1} [1 - e^{-(N-k)\sigma_\phi^2/2}] \\ &= \frac{1}{N} + \frac{2}{N^2} \frac{1}{e^{\sigma_\phi^2/2} - 1} \\ &\quad \cdot \left[(N-1) - \frac{1 - e^{-(N-1)\sigma_\phi^2/2}}{e^{\sigma_\phi^2/2} - 1} \right] \end{aligned} \tag{72}$$

where the second equality follows by recognizing that the sum over k is again a geometric series. To understand the implications of (72), we first consider the limit $\sigma_\phi \rightarrow 0$, for which the RHS of (72) $\rightarrow 1$, as expected for a perfect structure. Retaining the lowest nonvanishing order in σ_ϕ we find

$$\langle \hat{\eta} \rangle \approx 1 - \frac{(N - N^{-1})\sigma_\phi^2}{6} \tag{73}$$

so we see that the efficiency begins to drop rapidly when the variance for a single domain approaches $1/N$. If we assume that $\sigma_\phi^2 << 1$, but not necessarily that $N\sigma_\phi^2 << 1$, we find from (72)

$$\langle \hat{\eta} \rangle \approx \frac{4}{N\sigma_\phi^2} - \left(\frac{8}{N^2\sigma_\phi^4} - \frac{1}{6N^2} \right)(1 - e^{-N\sigma_\phi^2/2}). \quad (74)$$

In most cases of interest, N is large, while from (74) we see that the efficiency is small unless $N\sigma_\phi^2 < 1$, so we can usually neglect the $1/6N^2$ term in (74), which then gives the efficiency as a function of a single variable $N\sigma_\phi^2$. Making this assumption, and expanding (74) to lowest order in $N\sigma_\phi^2$, we find

$$\langle \hat{\eta} \rangle \approx 1 - \frac{\pi^2}{6} N \left(\frac{\sigma_l}{l_c} \right)^2 \quad (75)$$

where we have used (70) to express σ_ϕ in terms of σ_l.

Plots of $\langle \hat{\eta} \rangle$ using both the lowest order approximation, (75), and the more accurate form, (74), under the assumption $N >> 1$, and the exact form, (72), assuming $N = 100$, are given in Fig. 3. We see that there is negligible difference between (72) and (74) over the entire range plotted, while (75) is accurate only over a rather restricted range. From the plot, we see that the tolerance on the mean square error for >50% conversion is $N\sigma_\phi^2 < 5.11$, or with (70) for σ_ϕ,

$$\sigma_l / l_c < 0.72/\sqrt{N}. \quad (76)$$

We found in (72)–(75) the ensemble average of the conversion efficiency at the nominal operating point in the presence of random period errors. For perfect structures, such operation yields the highest conversion efficiency. However, as is discussed in Appendix II, in imperfect structures it is often possible to obtain higher conversion efficiency by tuning away from the nominal operating point through, for example, temperature, angle, or wavelength tuning. If one is interested in the maximum conversion efficiency irrespective of operating point, the analysis of Appendix II can be applied to obtain $\Delta k_0' + \delta\Delta k_{\text{opt}}'$ and $\hat{\eta}_{\text{opt}}$, the optimized operating point and the conversion efficiency at the operating point, respectively. As we are interested here in random errors, one can of course calculate only ensemble averages of these quantities. The statistical analysis proceeds in the same fashion as that presented for the nominal case above, but is rather more complicated. We present here only the results in the limit of large numbers of domains and small phase errors. We find

$$\langle \hat{\eta}_{\text{opt}} \rangle \approx 1 - \frac{N}{15}\sigma_\phi^2 = 1 - \frac{\pi^2}{15} N \left(\frac{\sigma_l}{l_c} \right)^2 \quad (77)$$

and

$$\langle \delta\Delta k_{\text{opt}}'^2 \rangle \approx \frac{6}{5}\frac{N}{L^2}\sigma_\phi^2 = \frac{6\pi^2}{5}\frac{N}{L^2}\left(\frac{\sigma_l}{l_c} \right)^2. \quad (78)$$

Note that the ensemble average of $\delta\Delta k_{\text{opt}}'$ vanishes, so that

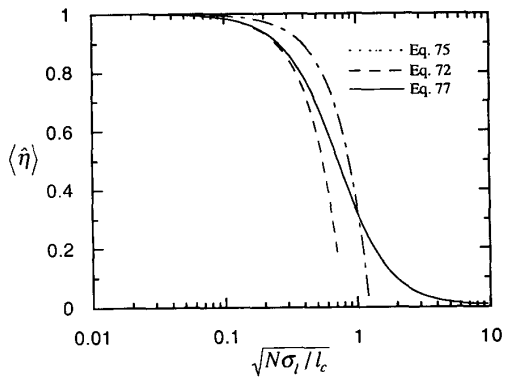

Fig. 3. Effect of random period errors on normalized SHG conversion efficiency, $\langle \hat{\eta} \rangle$. Solid curve is exact expression for Gaussian distribution of domain lengths [(71)] where the number of domains, $N = 100$; dashed curve is first approximated given in (75); dash-dotted curve is the approximation to the optimized efficiency given in (77). Here σ_l is the variance in the period, l_c is the coherence length, and N is the number of domains. The approximation given by (74) evaluated in the limit $N \to \infty$ is indistinguishable from the solid curve on the scale of this figure.

(78) gives the breadth of the distribution of optimum operating points centered around the nominal point. Comparing (77) with (75) as plotted in Fig. 3, we see that the optimized conversion efficiency decreases substantially more slowly with the magnitude of the period errors than does the nominal conversion efficiency, leading to an increase in the tolerance for the mean square error to $N\sigma_\phi^2 < 7.5$. Comparison of this tolerance calculated in the small error limit against numerical calculations valid for errors of arbitrary magnitude indicates that the actual tolerance is approximately 20% greater than that obtained from (77).

D. Linear Taper of Period

In the growth of periodically poled single-crystals, a slow drift in the crystal pull rate or in the modulation frequency of the boundary position can lead to a corresponding drift in the poling period along the length of a sample. Such a drift can be modeled by a linear taper of domain length. Let the total difference in domain length from one end of the sample to the other be Δl. For a sample containing N domains the error in length of the jth domain is then given by

$$\Delta l_j = \frac{\Delta l}{N}\left(j - \frac{N}{2} \right). \quad (79)$$

Here we have assumed that the domain at $j = N/2$ is of the ideal length. This condition does not in general produce the highest conversion efficiency for a given Δl (see Appendix II), but is close to the optimum and can be used to conveniently investigate the effect of varying the magnitude of Δl.

With (7), (61), and (79) we have the phase error at the kth boundary

$$\Phi_k = \frac{\pi}{l_c}\sum_{j=1}^{k}\delta l_j = \frac{\pi\Delta l}{2Nl_c}[k(k+1) - Nk]. \quad (80)$$

Rather than attempt to evaluate the sum in (9) for the output field, we assume that N is large and the phase error moderate so that we may apply the approximate integral expression given in (13), to find

$$\hat{E}_2 \approx \frac{1}{L}\int_0^L e^{-i\Phi(z)}\,dz \tag{81}$$

where the continuous function $\Phi(z)$ is chosen, according to (11), as

$$\Phi(z) = \frac{\pi\Delta l}{2Nl_c}\left[\left(\frac{z}{ml_c}\right)^2 - (N-1)\left(\frac{z}{ml_c}\right)\right]. \tag{82}$$

With (82), appropriate changes of variable allow us to cast (81) in the form

$$\hat{E}_2 = e^{i\pi\xi^2/2}\frac{1}{\xi}\int_0^{\xi} e^{-i\pi t^2/2}\,dt$$

$$= e^{i\pi\xi^2/2}\frac{1}{\xi}\left[C(\xi) - iS(\xi)\right] \tag{83}$$

where ξ is defined as

$$\xi \equiv \frac{1}{2}\sqrt{\frac{N\Delta l}{l_c}} \tag{84}$$

and in the second equation the result is expressed in terms of the Fresnel integrals defined in [42]. With (83), the normalized conversion efficiency is found to be

$$\hat{\eta}_{\text{tap per}} = \frac{1}{\xi^2}\left[C^2(\xi) + S^2(\xi)\right]. \tag{85}$$

A series expansion for small arguments of the Fresnel integrals gives

$$\hat{\eta}_{\text{tap per}} \approx 1 - \frac{\pi^2}{45}\xi^4 = 1 - \frac{\pi^2}{720}N^2\left(\frac{\Delta l}{l_c}\right)^2. \tag{86}$$

Equation (85) and its approximation (86) are plotted in Fig. 4 as functions of $\xi \equiv 1/2\sqrt{N\Delta l/l_c}$. From Fig. 4 we see that the normalized conversion efficiency drops to 50% when $\xi = 1.318$, so we can establish a tolerance for linear taper according to

$$\frac{\Delta l}{l_c} < \frac{6.95}{N}. \tag{87}$$

E. Quantization of Domain Boundary Positions

If the positions of the domain boundaries can take only certain discrete values, due perhaps to quantization in a fabrication process such as lithographic mask making, then the domain lengths will deviate somewhat from optimum. Let us take q to be the increment in domain length imposed by quantization, $\bar{l}$ to be the desired domain length (typically ml_c), and assume that $\bar{l} = (Q + \epsilon)q$, where Q is an integer and ϵ is a fraction such that $-1/2 < \epsilon < 1/2$. For simplicity we assume that $H \equiv 1/\epsilon$ is an even integer, though the conclusions we reach are generally valid as long as H is not too small.

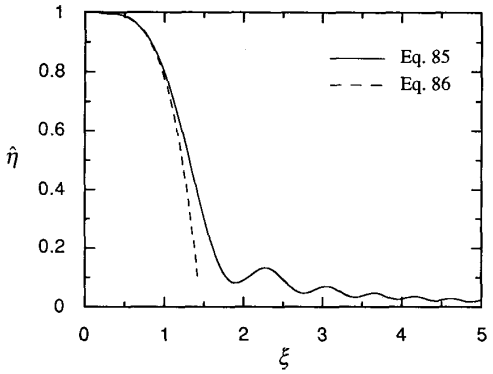

Fig. 4. Normalized conversion efficiency $\hat{\eta}$ as a function of the magnitude of the taper for a QPM device with linearly tapered domain thicknesses. Solid line is exact calculation of (85), dashed line is approximation given in (86). $\xi = \sqrt{N\Delta l/4l_c}$ is a measure of the taper Δl, normalized to the coherence length l_c and the number of domains N, as defined in (84).

The desired domain distribution is of course described by $z_{z,0} = j\bar{l}$. With the given parameters, we can construct an approximation to the desired structure that deviates by no more than $q/2$ from the desired structure, by placing one domain of length $(Q + \epsilon/|\epsilon|)q$ between H domains of length Qq, so that the structure is periodic with period $2P + 1$, where $2P = H/2$. Within such a section, the position error of the jth boundary varies linearly between $q/2$ and $-q/2$, so that we can take the position error to be

$$\delta z_{k+j} = jq/2P \qquad -P \le j \le P \tag{88}$$

where k is chosen such that $\delta z_k = 0$. In a structure of N domains, there will be $N_P = N/(2P)$ identical sections of this type.

To analyze the effect of such a periodic linear error, we turn to (9), modified to account for the periodic error

$$\hat{E}_2 = \frac{N_P}{N}\sum_{j=-P}^{P} e^{-i\Phi_j} \tag{89}$$

where the phase error, with (7) and (88) is given by

$$\Phi_j = (\Phi_M/P)j \tag{90}$$

where $\Phi_M = \Delta k'\, q/2$ and with no loss of generality we have taken $k = 0$. With (90), (89) can be recognized as a geometric series, which can be summed to yield

$$\hat{E}_2 = \frac{N_P}{N}\left[1 + 2\,\text{Re}\left(\frac{1 - e^{-i\Phi_M}}{e^{i\Phi_M/P} - 1}\right)\right]$$

$$= (1 + 2P)^{-1} \cdot \left\{1 + \frac{2\sin(\Phi_M/2)\cos\left[(1 + 1/P)\Phi_M/2\right]}{\sin(\Phi_M/2P)}\right\}$$

$$\approx \frac{1 + 2P\,\text{sinc}(\Phi_M)}{1 + 2P} \tag{91}$$

where the approximate form holds for $\Phi_M << 2P$.

For $P >> 1$, the conversion efficiency calculated ac-

cording to (91) goes as $\text{sinc}^2(\Phi_M)$, so in order that the efficiency remain within 50% of the ideal, we must have $\Phi_M < 0.443\,\pi$, or, with (90),

$$q/l_c < 0.89. \tag{92}$$

While (91) predicts an efficiency reduction of 1–10% for typical visible-light devices, one can in most cases compensate for the linearly increasing phase error by a small change in the phase mismatch $\Delta k'$, accomplished through a shift in the operating wavelength or temperature. The necessary shift in operating point $\delta\Delta k'$ to eliminate the phase shift, or equivalently the shift necessary to make the design length $\bar{l}$ an integral multiple of the quantization increment q, is

$$\frac{\delta\Delta k'}{\Delta k'} = \frac{q}{2P\bar{l}}. \tag{93}$$

F. Periodic Errors in Boundary Position

A common type of error in domain distribution is a periodic drift in the position of the boundaries, such as might be caused by oscillations in the position of the freezing boundary during growth of a periodically poled crystal. Such errors can be described as a phase modulation of the domains, according to

$$z_j = z_{j,0} + v \sin(\Omega z_{j,0}) \tag{94}$$

so that the phase error is, according to (7),

$$\Phi_j = \Delta k' v \sin(\Omega z_{j,0}). \tag{95}$$

Analyzing this problem according to (13), we find that the normalized output field is given by

$$\hat{E}_2 = \frac{1}{L}\int_0^L e^{-i\Delta k' v \sin(\Omega z)}\,dz. \tag{96}$$

Assuming for simplicity that $\Omega L/\pi$ is an integer, the RHS of (96) is a standard integral form of the Bessel function J_0, so that we have

$$\hat{E}_2 = J_0(\Delta k' v) \tag{97}$$

and the normalized efficiency is given by

$$\hat{\eta} = J_0^2(\pi v/l_c). \tag{98}$$

Note that this result holds independent of the magnitude of Ω and L so long as $\Omega L/\pi$ is an integer, and is a good approximation for any value of Ω satisfying $\Omega L >> 1$. The tolerance for 50% normalized conversion efficiency is quite strict:

$$v/l_c < 0.358. \tag{99}$$

IV. Phase-Matching Tuning Curves

In the previous section, the reduction of the peak efficiency for various nonideal structures was related to the magnitude of the errors. While these results are useful for establishing tolerances on the fabrication processes, for characterization of unknown errors one would prefer to have information on the shape of the tuning curves, as these are more easily measured than are absolute conversion efficiencies. In this section, we discuss the form of the tuning curves for the types of errors analyzed in the previous section. Similar calculations for conventionally phase-matched crystals are discussed in [43]. We also briefly present techniques for synthesizing desired tuning curves by appropriate modulation of the domain structure. To simplify these analyses of the tuning curves, we assume throughout that the number of domains is large enough that the approximate integral expression for the output field, (13), is accurate.

A. Effects of Various Errors on SHG Tuning Curves

Consider first the random errors described in Section III-B. With (13) for the field, we obtain for the normalized intensity

$$\hat{\eta} = \frac{1}{L^2}\int_0^L dz \int_0^L dz' e^{-i[\Phi(z) - \Phi(z')]}. \tag{100}$$

This double integral can be manipulated similarly to the double sum in (52), to yield

$$\begin{aligned}\langle \hat{\eta} \rangle &= \frac{2}{L^2}\int_0^L dz \int_0^{L-z} ds\, \langle \cos[\Phi(z+s) - \Phi(z)] \rangle \\ &= \frac{2}{L^2}\int_0^L dz \int_0^{L-z} ds\, \langle \cos[\Delta\Phi(z,s)] \rangle \end{aligned} \tag{101}$$

where $s = z' - z$, and $\Delta\Phi(z, s) = \Phi(z + s) - \Phi(z)$. According to (65) and (11),

$$\langle \cos[\Delta\Phi(z,s)] \rangle = e^{-\sigma^2_{\Delta\Phi}(s)/2} \cos[\langle \Delta\Phi(s) \rangle] \tag{102}$$

where, according to (63) and (11),

$$\langle \Delta\Phi(s) \rangle = \delta\Delta k' s \tag{103}$$

and,

$$\sigma^2_{\Delta\Phi}(s) = \begin{cases} \sigma_\phi^2 & \text{duty cycle errors} \\ \sigma_\phi^2 s/ml_c & \text{period errors} \end{cases} \tag{104}$$

where $\sigma_\phi^2 = (\pi\sigma_l/l_c)^2$.

For random duty cycle erorrs, the double integral obtained from (101), (102), and (104) is easily evaluated, yielding

$$\langle \hat{\eta} \rangle = e^{\sigma_\phi^2/2}\,\text{sinc}^2(\delta\Delta k' L/2). \tag{105}$$

We see that in this case the width of the tuning curve is unaffected, with the ordinary sinc dependence scaled by an overall efficiency factor, a result of the nonaccumulating nature of the phase errors for this type of random function.

For random period errors, evaluation of the double integral obtained from (101), (102), and (104) is rather more complicated, ultimately yielding

$$\begin{aligned}\langle \hat{\eta} \rangle = 2D^{-2}\{&F^2 - S^2 + SD + e^{-S} \\ &\cdot [(S^2 - F^2)\cos(F) - 2FS\sin(F)]\}\end{aligned} \tag{106}$$

where

$$F = \delta\Delta k'L$$
$$S = N\sigma_\phi^2/2$$
$$D = F^2 + S^2. \tag{107}$$

In this case the width of the curve increases with σ_ϕ, because of the accumulation of phase error in a random walk fashion. The normalized efficiency as a function of mismatch F for several values of S is shown in Fig. 5, where the transition from a sinc^2 $(F/2)$ dependence for a perfect structure to a broadened curve with the periodic features washed out is clear. From (106) it can be shown that $\langle\eta\rangle \rightarrow 2S^{-1}(1 - S^{-1})$ and that the FWHM $2F_{1/2} \rightarrow 2S(1 + S^{-1})$ asymptotically for large S. These results can be explained qualitatively in terms of a model considering the output field to be the incoherent sum of the contributions of M sections of length l_{eff}, where $M = L/l_{\text{eff}}$, and $l_{\text{eff}} = l_c^3/2\sigma_l^2$ is the length over which the error in the boundary position "randomly walks," a distance $l_c/\sqrt{2}$. This choice of l_{eff} leads to results for the efficiency and the phase-matching bandwidth (calculated as $\delta\Delta k'_{\text{FWHM}} = 2\pi/l_{\text{eff}}$) within 20% of the correct value.

It should be noted that the tuning curve of a particular curve device chosen from an ensemble with a given S does not necessarily resemble the ensemble average of the tuning curves. This observation is true even for large N, because the contributions of a relatively small number M of "coherent sections" add to one another to produce the output field. The breadth of the ensemble average of the tuning curves is in large part due to the distribution of peak detunings (78) rather than the breadth of the individual tuning curves. A quantity that would bear a closer resemblance to a typical tuning curve would be the ensemble average of $\hat{\eta}$ as a function of the detuning from the *optimum* value of $\delta\Delta k'$ [(77)–(78)]. Numerical simulations suggest that individual tuning curves deviate significantly from even this latter quantity, so we do not reproduce the calculation here.

We now consider the linearly tapered period error discussed in Section III-D. To include frequency tuning, the phase function of (82) is modified according to (7) yielding

$$\Phi(z) = \frac{\pi\Delta l}{2Nl_c}\left[\left(\frac{z}{ml_c}\right)^2 - (N-1)\left(\frac{z}{ml_c}\right)\right] + \delta\Delta k'z. \tag{108}$$

Inserting this function into (13) for E_2, carrying out an analysis similar to that leading to (83), and finding the square magnitude of the result, we obtain

$$\hat{\eta} = \frac{1}{4\xi^2}\left(\{C[\xi(1+\nu)] + C[\xi(1-\nu)]\}^2 + \{S[\xi(1+\nu)] + S[\xi(1-\nu)]\}^2\right) \tag{109}$$

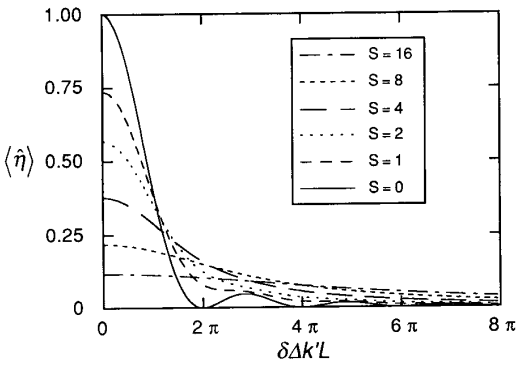

Fig. 5. Normalized SHG efficiency $\langle\hat{\eta}\rangle$ for QPM devices with random period errors versus the detuning from nominal phase-matching, $\delta\Delta k'L$. The curves are parameterized by $S = N\sigma_\phi^2/2$, a measure of the randomness defined in (107).

where ξ was defined in (84) and ν is defined as

$$\nu = \frac{2l_c}{\pi N\Delta l}\delta\Delta k'L = \frac{1}{2\pi\xi^2}\delta\Delta k'L. \tag{110}$$

The function defined in (109) is essentially the same as the result for Fresnel diffraction from a single slit, with ξ^2 playing the role of the Fresnel number and ν the transverse position.

Tuning curves are plotted according to (109) for several values of ξ in Fig. 6. For cases where FWHM conversion peak is broad compared to that of an ideal structure, i.e., for $\xi^2 >> 1$, the peak efficiency occurs for $\nu \approx 1$, and the product of the peak efficiency and the FWHM is approximately constant. Note that if the efficiency for the optimum ν were plotted in Fig. 4 rather than the efficiency for $\nu = 0$, the overall decrease with ξ would be similar, but the strong ripples would be eliminated.

Finally, we turn to the case of periodic errors in the position of the boundaries, as discussed in Section III-F. Phase mismatch is included by modifying (95) according to (7) to obtain

$$\Phi(z) = \Delta k'v \sin(\Omega z) + \delta\Delta k'z. \tag{111}$$

Inserting this result into the integrand to (81), applying the standard Bessel function expansion of the complex exponential, evaluating the integral, and squaring the result, we find

$$\hat{\eta} = \left| J_0(\Delta k'v)\,\text{sinc}(u) + \sum_{p=1}^{\infty} J_p(\Delta k'v) \cdot [e^{ipR}\,\text{sinc}(u + pR) + (-1)^p e^{-ipR}\,\text{sinc}(u - pR)]\right|^2 \tag{112}$$

where $u = \delta\Delta k'L/2$ and $R = \Omega L/2$. The normalized efficiency as a function of phase mismatch for $R = 3\pi$ is plotted in Fig. 7 for several values of the domain boundary errors $v/l_c = \Delta k'v/\pi$. We see that the effect of the phase modulation is to induce sidebands on the phase-

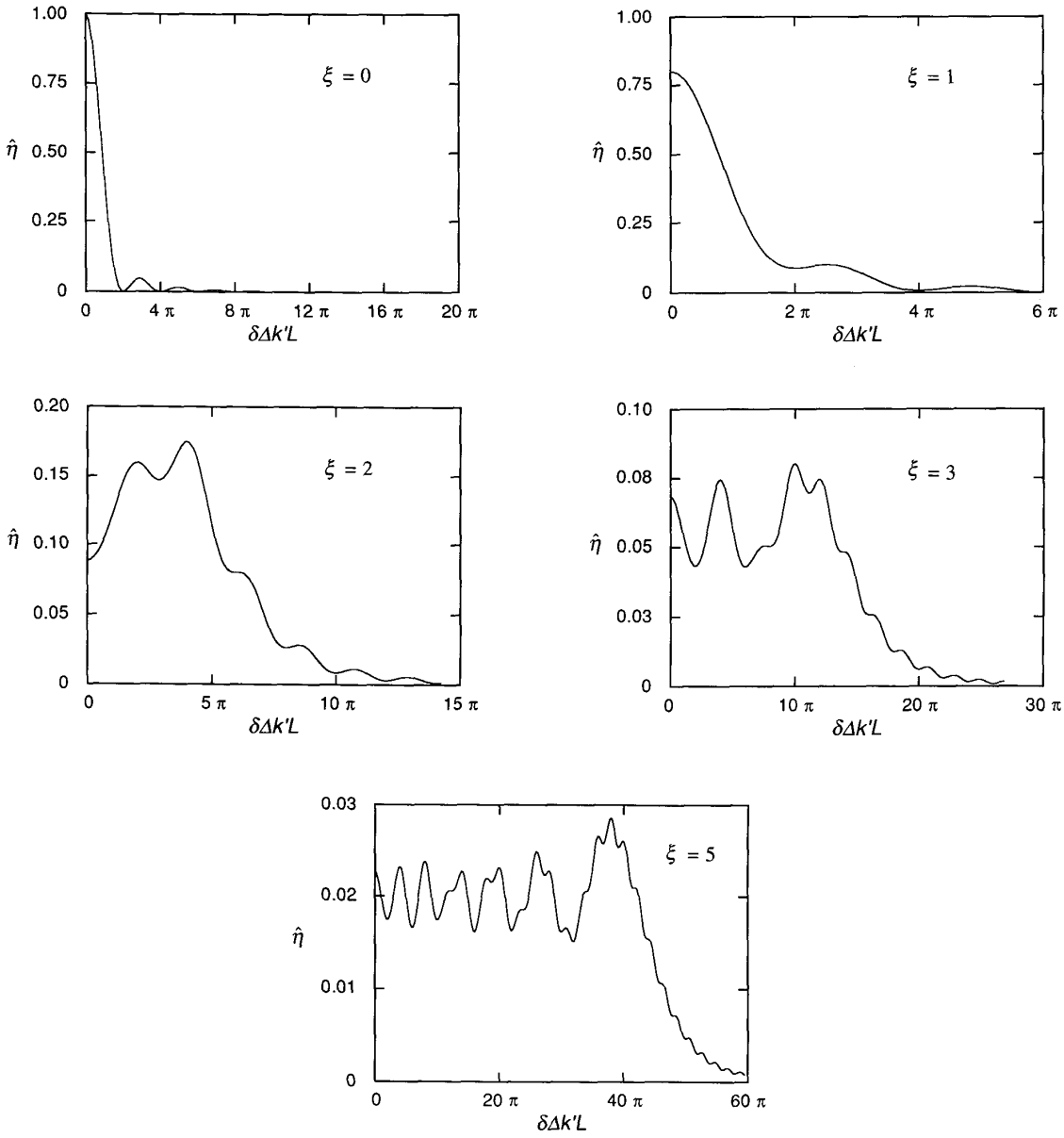

Fig. 6. Normalized SHG conversion efficiency $\hat{\eta}$ for QPM devices with linearly tapered domain widths vs the detuning from nominal phase matching $\delta\Delta k'L$. $\xi = \sqrt{N\Delta l/4l_c}$ is a measure of the taper, defined in (84).

matching curve, so that a series of sinc^2 functions with centers shifted by the modulation frequency are obtained. Note that the width of the peaks is dictated only by the length of the crystal, and is independent of the phase modulation amplitude, consistent with the phase coherency of the domains over the whole structure. Of course, the amplitude of the largest peak decreases with increasing modulation depth. For $R < 1$, the separation of the sidebands is smaller than the width of the sinc^2 curve, so the effect of the modulation is to broaden and lower the central peak.

B. Synthesis of Tuning Curves

It would frequently be useful to be able to exert some control over the phase-matching properties of a nonlinear optical device, for example to broaden its phase-matching bandwidth. We have seen in the previous section how various types of errors in the periodicity of a quasi-phase-matching structure can lead to alteration and broadening of the phase-matching curves. More desirable, however, would be the ability to completely specify the shape of the tuning curve. Because of the Fourier transform relationship between the tuning curve and the longitudinal

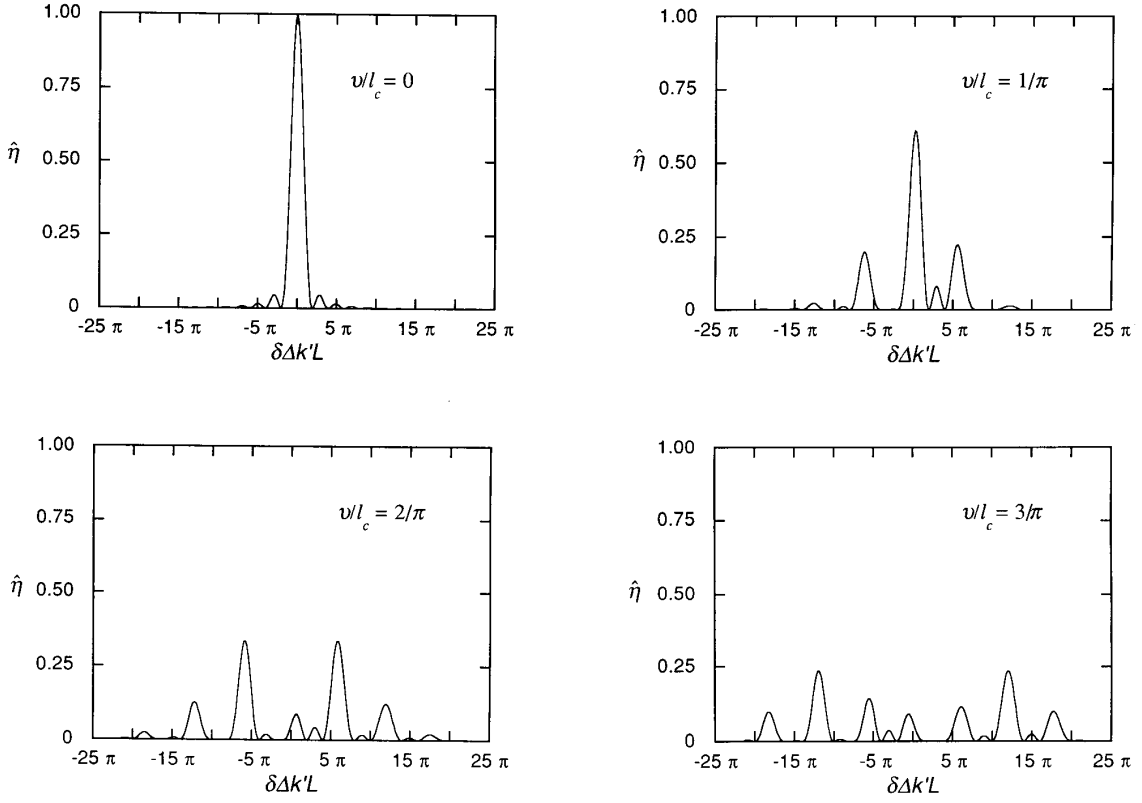

Fig. 7. Normalized SHG conversion efficiency $\hat{\eta}$ for QPM devices with periodically varying domain widths versus the detuning from nominal phase matching, $\delta\Delta k'L$. v is the amplitude of the modulation, as defined in (108). Spatial frequency of the modulation is $\Omega = 6\pi/L$.

profile of the nonlinear coefficient [(16)], it would in principle suffice to specify the nonlinear coefficient profile as the inverse transform of the desired tuning curve. However, a method does not exist for continuously varying the magnitude of the nonlinear coefficient in most materials. With QPM, one can use a programmed sequence of domain reversals to approximate the desired control. Note that the Fourier transform relation between the generated field $E_2(\Delta k)$ and the nonlinear coefficient profile $g(z)$ limits the maximally achieved conversion efficiency. In the common case where $g(z)$ only takes on the values $+1$ and -1, the generated power of the second harmonic integrated over the phase-mismatch, i.e., the area under the phase-matching curve, is independent of $g(z)$. Thus, a broadening of the phase-matching width will result in a reduced peak efficiency.

As an approach for constructing a discrete approximation to a desired nonlinear coefficient profile, consider a "building block" consisting of two consecutive domains having the opposite sign of nonlinear coefficient, each of magnitude d_{eff}, as illustrated in Fig. 8. The total length of the block is $\mathcal{L}$ (ideally chosen to be $2ml_c$), the length of the first domain is l, and thus the length of the other is $\mathcal{L} - l$. The increment in the second-harmonic field after one such block is found using (4) to be

$$E_2 = \frac{\Gamma d_{\text{eff}}}{-i\Delta k'}\left[(e^{-i\Delta k' l} - 1) - (e^{-i\Delta k'\mathcal{L}} - e^{-i\Delta k' l})\right]$$
$$= \frac{2\Gamma d_{\text{eff}}}{\Delta k'}\left[2e^{-i\Delta k' l/2}\sin(\Delta k' l/2) - e^{-i\Delta k'\mathcal{L}/2}\sin(\Delta k'\mathcal{L}/2)\right]. \quad (113)$$

The field generated by this building block is equal to that generated in a single phase-matched layer of the same thickness with an equivalent nonlinear coefficient d_Q. Comparing (113) with the field generated in such a homogeneous layer $E_2 = \Gamma\mathcal{L}d_Q$ we see that

$$d_Q = \frac{2d_{\text{eff}}}{\Delta k'\mathcal{L}}\left[2e^{-i\Delta k' l/2}\sin(\Delta k' l/2) - e^{-i\Delta k'\mathcal{L}/2} \cdot \sin(\Delta k'\mathcal{L}/2)\right] \quad \text{for arbitrary } \mathcal{L})$$
$$= \frac{2d_{\text{eff}}}{m\pi}e^{-i\Delta k' l/2}\sin(\Delta k' l/2) \quad (\text{for } \mathcal{L} = 2ml_c). \quad (114)$$

Thus, the magnitude and the phase of the equivalent non-

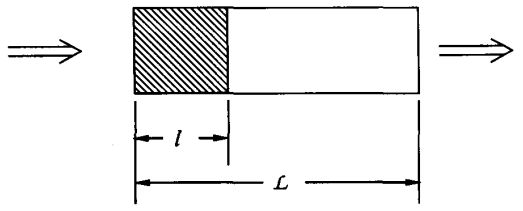

Fig. 8. Schematic of a building block for tuning curve synthesis. Shaded area represents a domain reversed in polarity from the rest of the block.

linear coefficient can be controlled by varying l, i.e., for a block with $l = l_j$,

$$\begin{cases} |d_{Q_j}| = \dfrac{2d_{\text{eff}}}{m\pi} |\sin(\Delta k' l_j/2)| \\ \angle d_{Q_j} = \pm \Delta k' l_j/2 \end{cases} \tag{115}$$

where the choice of the sign of the phase is given by $-\text{sgn}[\sin(\Delta k' l_j/2)]$. Note that the simple form for d_{Qj} in (115) is based on the second form of (114), and hence is not strictly valid when tuning away from $\Delta k = 0$, because the block length $\mathcal{L}$, which physically stays the same, departs from $2ml_c$ through the change in l_c.

A structure which possesses the desired phase-matching tuning curve can be built up by stacking a series of these building blocks, with the magnitudes of their effective nonlinear coefficients describing a profile which is a discrete approximation to the inverse Fourier transform of the desired tuning curve. (That the intensity tuning curve is the square of the Fourier transform of the d_{Qj} must of course also be taken into account.) We will consider here the case in which all of the blocks in the device structure are of the same length. Negative values of d_Q may be achieved in either of two ways. The signs of both domains in the building block can be reversed, or values of l_j which make $\sin(\Delta k' l_j/2)$ negative can be used if $m > 1$. Numerical modeling seems to indicate better tuning behavior in structures using the former technique. It also indicates that some ranges of l are better than others in obtaining well-formed tuning curves. Note that increasing m can increase the minimum necessary domain length, but the tolerance on errors in the positions of the domain boundaries remains the same.

Tuning curves approximating a rectangle function and a triangle function generated by approximating the inverse transforms with 128 blocks with $m = 3$ and with l running from $2l_c$ to $3l_c$ are shown in Fig. 9(a) and (b), respectively. Sign changes necessary in the sinc function with three sidelobes on each side of the origin used as the inverse transform for Fig. 9(a) were obtained by reversing the polarity of the relevant blocks. Heights of the synthesized tuning curves are normalized in the figure to the peak efficiency of an "ideal" QPM structure of the same total length L and the same order ($m = 3$) but with $d_{Qj} = 2d_{\text{eff}}/m\pi$ (independent of j). The abscissa in the figure is in units of the half width of the first zero of the same "ideal" tuning curve. The shorter effective length of the

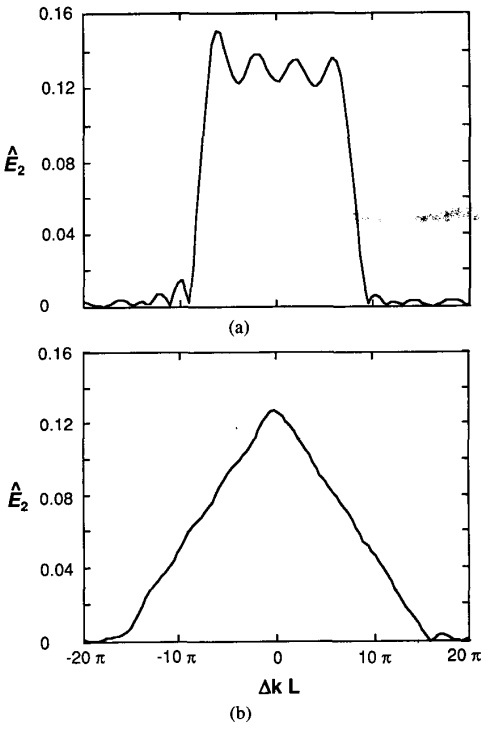

Fig. 9. Synthesized tuning curves using the "building block" method with $m = 3$ in a structure of length Nl_c. (a) Rectangular tuning curve synthesized using $d_{Qj} = \text{sinc}(24\pi j/N)$. (b) Triangular tuning curve synthesized using $d_{Qj} = \text{sinc}^2(24\pi j/N)$. Amplitudes are normalized to the peak of the tuning curve for an "ideal" quasi-phase-matched structure of the same total length L and the same order $m = 3$, but with d_{Qj} = constant. The abscissa is in units of the half width to the first zero of the same "ideal" tuning curve.

structures leads to a factor of four increase in the width of the tuning curve and a proportional reduction in the peak conversion, which is the price one must pay to tailor the tuning-curve shape. The slight asymmetry and presence of small ripples on the curves are effects caused by the nonuniform phase of the structures. The severity and handedness of these phase effects were found to depend on the range of l used in synthesizing the profiles. As expected, tuning curves having the same shape are calculated in real space [(3)] and Fourier space (a fast Fourier transform evaluation of (16) on the complex spatially varying nonlinear coefficient obtained from (114)).

The complication of nonuniform phase during tuning prevents the attainment of truly arbitrary tuning curves. Best results are obtained in synthesizing phase-matching functions which are symmetrical (even) about $\Delta k = 0$. Independent control of both magnitude and phase of the effective nonlinear coefficient is not possible with the simple building block proposed above. It is possible to construct more complicated building blocks for which the phase is the same regardless of the magnitude at a fixed $\Delta k'$, but since the phase across domains of different lengths tunes at different rates, it does not appear to be possible to form a truly phase-compensated structure. Nevertheless, the class of tuning curves which can be successfully synthesized contain many useful members.

The synthesis method outlined above represnts an example of what Nazarathy *et al.* [38], [44], [45] have called an "analog" approach to the design of phase reversal structures. Optimization algorithms such as that used by Erasme *et al.* [46] might be used to improve the performance of a structure synthesized with the present technique by making adjustments to the positions of domain reversals. A "digital" approach may also be taken, in which domain lengths are only allowed to take values which are multiples of a minimum "chip" length. If the objective is to maximize the bandwidth, with conversion efficiency being of subsidiary importance, Nazarathy has shown that by using suitable digital pseudorandom sequences such as Barker codes, bandwidths approaching that of a sample a single chip long can be obtained without the conversion efficiency falling to that of a single chip.

V. Simultaneous Linear and Nonlinear Modulation

In experimental implementations of QPM, modulation of the linear optical properties of the medium often occurs, either as an unintended byproduct of the domain inversion process, or intentionally as a means for accomplishing QPM. To analyze such devices, (1) for the evolution of the second harmonic field must be modified to

$$\frac{dE_2}{dz} = \gamma \frac{d(z)}{n_1(z)n_2(z)} e^{-i\phi(z)} \tag{116}$$

where the phase error $\phi(z)$ is given by

$$\phi(z) = \int_0^z \Delta k'(z')\, dz' \tag{117}$$

$\gamma = i2\omega I_1/c^2\epsilon_0$, and I_1 is the intensity at the fundamental. Consider a structure consisting of N layers, with the nth layer extending from z_{n-1} to z_n. Assuming the properties of the medium are homogeneous within each layer, we can integrate (116) to obtain

$$E_2(z_n) = i\gamma \sum_{j=1}^{n} \xi_j (e^{-i\phi_j} - e^{-i\phi_{j-1}}) \tag{118}$$

where

$$\phi_j = \sum_{i=1}^{j} \Delta\phi_i \tag{119}$$

$$\Delta\phi_j = \Delta k_j' (z_j - z_{j-1}) \tag{120}$$

and

$$\xi_j = \frac{d_j}{n_{1,j}n_{2,j}\Delta k_j'}. \tag{121}$$

Evaluating (118) at the output of the device ($z = z_N$), and reindexing the second sum, we find

$$E_2(z_N) = i\gamma \sum_{j=1}^{N-1} (\xi_j - \xi_{j+1}) e^{-i\phi_j} + i\gamma(\xi_N e^{-i\phi_N} - \xi_1)$$

$$\approx i\gamma \sum_{j=1}^{N} (\xi_j - \xi_{j+1}) e^{-i\phi_j} \tag{122}$$

where the approximate form neglects a contribution approximately equal to that of a single layer, and should be accurate when N is large, similar to (9).

To make further progress, we must make further assumption about the nature of the modulation of the medium. In the simplest case of interest, the medium consists of two alternating types of layers. We can then write the material parameter ξ_j as

$$\xi_j = \bar{\xi} + (-1)^j \Delta\xi_j \tag{123}$$

where $\bar{\xi}$ is the mean of ξ and $2\Delta\xi_j$ is the peak to peak modulation. The subscript j is retained on $\Delta\xi_j$ to allow for nonideal structures in which the modulation depth is not constant along the length of the device. With (123), the approximate form of (122) becomes

$$E_2(z_N) \approx i2\gamma \sum_{j=1}^{N} \Delta\xi_j (-1)^j e^{-i\phi_j}. \tag{124}$$

If we further assume that the device is designed for symmetrical odd order QPM, i.e., that each layer is nominally an odd number of coherence lengths long, and define a phase error Φ_j to account for errors in the domain spacing, (124) can be written

$$E_2(z_N) \approx i2\gamma \sum_{j=1}^{N} \Delta\xi_j e^{-i\Phi_j} \tag{125}$$

where $\phi_j = jm\pi + \Phi_j$, and m is an odd integer.

If the modulation depth is constant over the length of the device, and the domains are all of the nominal length ml_c, (125) becomes simply

$$E_2(z_N) = i2\gamma\Delta\xi N. \tag{126}$$

Comparing (126) with the solution to (116) for a homogeneous conventionally phase-matched medium, $E_2(L) = \gamma d_{\text{eff}} L/n_1 n_2$, we see that the modulated medium generates the same output field as would a homogeneous medium with a nonlinear susceptibility d_{equiv}, given by

$$d_{\text{equiv}} = i2n_1 n_2 \Delta\xi \frac{N}{L}. \tag{127}$$

To understand the implications of this result, consider several special cases. For ordinary QPM, the indices of refraction are not modulated, but the nonlinear coefficient is modulated by $\pm d_{\text{eff}}$. We then have, with (121) and (123), $\Delta\xi = d_{\text{eff}}/(n_2 n_1 \Delta k')$, and $N = L/(ml_c)$, so with (127) we obtain $d_{\text{QPM}} = (2/m\pi) d_{\text{eff}}$, in agreement with (10).

If the indexes of refraction are modulated, we have "grating assisted phase matching" (GAPM) [26], [27],

[28], [30]. Taking the indexes of refraction to be

$$n_1 = \bar{n}_1 + \Delta n_1 \quad \text{and} \quad n_2 = \bar{n}_2 \pm \Delta n_2, \tag{128}$$

$\Delta\xi$ and N are given by

$$\begin{aligned}\Delta\xi &= \frac{d_{\text{eff}}\lambda\bar{n}_1\bar{n}_2}{4\pi}\,\frac{\Delta n_2(2-\bar{n}_1/\bar{n}_2)-\Delta n_1(2-\bar{n}_2/\bar{n}_1)+\Delta n_2\Delta n_1(\Delta n_2-\Delta n_1)/(\bar{n}_1\bar{n}_2)}{(\bar{n}_1^2-\Delta n_1^2)(\bar{n}_2^2-\Delta n_2^2)[(\bar{n}_2-\bar{n}_1)^2-(\Delta n_2-\Delta n_1)^2]} \\ &\approx \frac{d_{\text{eff}}\lambda}{4\pi}\,\frac{\Delta n_2(2-\bar{n}_1/\bar{n}_2)-\Delta n_1(2-\bar{n}_2/\bar{n}_1)}{\bar{n}_1\bar{n}_2(\bar{n}_2-\bar{n}_1)^2} \\ &\approx \frac{d_{\text{eff}}\lambda}{4\pi}\,\frac{\Delta n_2-\Delta n_1}{\bar{n}_1\bar{n}_2(\bar{n}_2-\bar{n}_1)^2}\end{aligned} \tag{129}$$

and

$$N = \begin{cases}\dfrac{4L(\bar{n}_2-\bar{n}_1)}{m\lambda}\left[1-\dfrac{(\Delta n_2-\Delta n_1)^2}{(\bar{n}_2-\bar{n}_1)^2}\right] \approx \dfrac{4L(\bar{n}_2-\bar{n}_1)}{m\lambda} & \text{if } |\bar{n}_2-\bar{n}_1| \geq |\Delta n_2-\Delta n_1| \\ \dfrac{4L(\Delta n_2-\Delta n_1)}{m\lambda}\left[1-\dfrac{(\bar{n}_2-\bar{n}_1)^2}{(\Delta n_2-\Delta n_1)^2}\right] \approx \dfrac{4L(\Delta n_2-\Delta n_1)}{m\lambda} & \text{if } |\bar{n}_2-\bar{n}_1| < |\Delta n_2-\Delta n_1|\end{cases} \tag{130}$$

where the first approximate form of (129) neglect terms of second order in Δn_1 and Δn_2, and the third form of (129) neglects terms second order in Δn or $(\bar{n}_2 - \bar{n}_1)$. To obtain (130) for N, the difference in the lengths of the domains due to the differences in the indexes of refraction must be taken into account. The first form of (130) holds for the case where the sign of the phase-mismatch $\Delta k'$ is constant throughout the crystal, whereas the second form assumes that $\Delta k'$ changes sign between neighboring domains. With (129) and (130), we find from (127) that

$$d_{\text{GAPM}} = i\,\frac{2d_{\text{eff}}}{m\pi}\,\frac{\Delta n_2-\Delta n_1}{\bar{n}_2-\bar{n}_1} \tag{131}$$

where only the form resulting from the lowest order approximations with $|\bar{n}_2 - \bar{n}_2| \geq |\Delta n_2 - \Delta n_1|$ is reproduced here. We see that the effective nonlinearity is smaller than that for QPM by the ratio of the dispersion modulation to the average dispersion.

If there is enough modulation in $\Delta k'$ to accomplish $\Delta n_2 = \Delta n_1$ with $\bar{n}_2 = \bar{n}_1$, it follows from (129) and (130) that $d_{\text{equiv}} = 2d_{\text{eff}}/m\pi = d_{\text{QPM}}$. In this special case, known as balanced phase matching (BPM) [29], the average phase-mismatch vanishes, and it is no longer necessary that the domain lengths be multiples of the coherence length. In the limit that the domain lengths are small compared to the coherence length, $d_{\text{BPM}} = d_{\text{eff}}$.

If both linear and nonlinear modulation are present, the situation is more complicated. Assume d_{eff} is given by $d_{\text{eff}} = \bar{d} \pm \Delta d$. If d_{eff} is modulated 100%, i.e., if $\bar{d} = 0$, the linear modulation has no first-order effect on the efficiency. If, on the other hand, the dispersion and both the linear and nonlinear modulation are small, we find from (121), (123), and (128) that

$$\Delta\xi \approx \frac{\bar{d}\lambda}{4\pi\bar{n}_1\bar{n}_2(\bar{n}_2-\bar{n}_1)}\left(\frac{\Delta d}{\bar{d}}-\frac{\Delta n_2-\Delta n_1}{\bar{n}_2-\bar{n}_1}\right) \tag{132}$$

where only first order terms in the modulation and the dispersion are retained. With (130) for N, we obtain from (126) and (127) $d_{\text{GAPM}} \approx (i2\bar{d}/m\pi)[\Delta d/\bar{d} - (\Delta n_2 - \Delta n_1)/(\bar{n}_2 - \bar{n}_1)]$. We see that depending on the relative phase of the linear and nonlinear modulations, their effects can add either constructively or destructively. For arbitrary magnitudes of linear and nonlinear modualtion, an expression similar to that of (129) can be obtained from (121), but the result is not presented here.

If the modulation is uniform, but phase errors exist, (125) takes the form

$$E_2(z_N) \approx i2\gamma\Delta\xi\sum_{j=1}^{N} e^{-i\Phi_j}. \tag{133}$$

Note that the summation in (133) is identical to that in (9) for ordinary QPM, so all the conclusions reached in Sections III and IV regarding the effects of various types of phase errors on the conversion efficiency carry over directly to GAPM. As an example, consider the effect of changing the duty cycle of the domains from the ideal of $m\pi$ for each layer. The structure then consists of alternate layers with phase shifts $\Delta\phi_a$ and $2\pi m - \Delta\phi_a$. Following (125), we then see that the phase error Φ alternates between $\Phi = m\pi - \Delta\phi_a$ and $\Phi = 0$. Noting that this type of error leaves the number of domains unchanged at the value given by (130) for a given length L, we find with (133)

$$E_2(z_N) \approx -2\gamma\Delta\xi N e^{-i\Delta\phi_a/2}\sin(\Delta\phi_a/2). \tag{134}$$

Comparing with the results for the ideal case $\Delta\phi_a = \pi m$ given in (126), we see that the magnitude of the effective nonlinear coefficient is reduced from the ideal by a factor $\sin(\Delta\phi_a/2)$, in agreement with (22) for ordinary QPM. It can similarly be shown that the results for even order GAPM are also analogous to those for conventional QPM.

We have to this point analyzed devices with abrupt boundaries between regions of different linear or nonlinear properties. This description is appropriate for many important systems, e.g., thin ferroelectric domain walls

in $LiNbO_3$ or index variations created by highly anisotropic diffusion in $KTiOPO_4$, but may not accurately describe other interesting systems where the material properties change more slowly with z. For the simplest form of such a continuous variation, the material parameters are sinusoidal functions of position, and we can write (116) as

$$\frac{dE_2}{dz} = \gamma \Xi(z)\, e^{-i\phi(z)} \tag{135}$$

where the combination of material parameters Ξ is given by

$$\Xi(z) \equiv \frac{d(z)}{n_1(z)n_2(z)} = \bar{\Xi} + \tilde{\Xi}\cos(Kz + \phi_\Xi). \tag{136}$$

Assuming $\Delta k'(z) = \overline{\Delta k'} + \Delta\tilde{k}'\cos(Kz + \phi_K)$, we obtain $\phi(z)$ with (117) as

$$\phi(z) = \overline{\Delta k'}z + (\Delta\tilde{k}'/K)\sin(Kz + \phi_K) - (\Delta\tilde{k}'/K)\sin(\phi_K). \tag{137}$$

Using (128), relations similar to (129) or (132) can be developed to relate Ξ and $\Delta k'$ to the modulation of the indexes of refraction and the nonlinear coefficient. The result is straightforward, and we do not reproduce the general term here. Note that the form assumed for Ξ in (136) contains only the fundamental modulation frequency, and hence is appropriate only when the amplitudes of the modulations are sufficiently small that higher order terms are not significant. No such restriction applies to (137), because $\phi(z)$ is a linear function of the index modulation. Inserting (136) and (137) in (135), expanding the phase-modulated exponential with the standard Bessel function series, and integrating the resulting series, we obtain

$$\begin{aligned} E_2(L) &= -i\gamma L e^{i(\Delta\tilde{k}'/K)\sin(\phi_K)} \\ &\quad \cdot \sum_{M=-\infty}^{\infty} (-1)^M e^{iM\phi_K}[\bar{\Xi}J_M \\ &\quad - \tfrac{1}{2}\tilde{\Xi}\{[(J_{M-1} + J_{M+1})\cos(\phi_\Xi - \phi_K) \\ &\quad + i(J_{M-1} - J_{M+1})\sin(\phi_\Xi - \phi_K)]\}]h_M(\overline{\Delta k'}) \\ &= -i\gamma L e^{i(\Delta\tilde{k}'/K)\sin(\phi_K)} \\ &\quad \cdot \sum_{M=-\infty}^{\infty} (-1)^M e^{iM\phi_K}[\bar{\Xi}J_M - \tilde{\Xi}[(MK/\Delta\tilde{k}')J_M \\ &\quad \cdot \cos(\phi_\Xi - \phi_K) \\ &\quad + iJ'_M \sin(\phi_\Xi - \phi_K)]]h_M(\overline{\Delta k'}) \end{aligned} \tag{138}$$

where the J_M are Mth order Bessel functions of the first kind evaluated at argument $(\Delta\tilde{k}'/K)$, J'_M is the derivative of the Bessel function with respect to argument, the phase-matching function h_M is defined as

$$h_M(\overline{\Delta k'}) = e^{-i[(\overline{\Delta k'} - MK)L/2]}\,\mathrm{sinc}\,[(\overline{\Delta k'} - MK)L/2] \tag{139}$$

and the second form of (138) follows from the first by standard recursion relations. Typically, only one frequency component will be close enough to phase matching to contribute significantly to the total field.

We can define an effective nonlinear coefficient for the Mth component of a sinusoidally modulated medium by comparing (138) to the result for an ideal homogeneously phase-matched crystal. We find

$$\begin{aligned} d_{SM} &= i(-1)^{M+1} e^{i[(\Delta\tilde{k}'/K)\sin(\phi_K) + M\phi_K]} \\ &\quad \cdot \bar{n}_1\bar{n}_2[\bar{\Xi}J_M - \tilde{\Xi}[(MK/\Delta\tilde{k}')J_M\cos(\phi_\Xi - \phi_K) \\ &\quad + iJ'_M \sin(\phi_\Xi - \phi_K)]] \end{aligned} \tag{140}$$

The effective nonlinear coefficient depends on both modulation depths, and their relative phase, as was seen for the discrete layer case. We can again best understand this result by examining various special cases. Consider the $M = 0$ and $M = 1$ terms:

$$\begin{aligned} |d_{SM,0}| &= \bar{n}_1\bar{n}_2|\bar{\Xi}J_0 + i\tilde{\Xi}J_1 \sin(\phi_\Xi - \phi_K)| \\ &\approx \bar{d}_{\mathrm{eff}}J_0 \\ |d_{SM,1}| &= \bar{n}_1\bar{n}_2|\bar{\Xi} - \tilde{\Xi}(K/\Delta\tilde{k}')\cos(\phi_\Xi - \phi_K)] \\ &\quad \cdot J_1 - i\tilde{\Xi}J'_1 \sin(\phi_\Xi - \phi_K)| \\ &\approx \bar{d}_{\mathrm{eff}}J_1. \end{aligned} \tag{141}$$

In both these expressions, the second form follows from the first under the assumption that $\tilde{\Xi} \ll (\Delta\tilde{k}'/K)$. For $M = 0$, the average phase-mismatch vanishes, and we have a situation similar to BPM. We see that achieving phase-matching through modulation around the mean reduces the effective nonlinear coefficient compared to ideal phase-matching in a homogeneous medium by a factor $J_0(\Delta\tilde{k}'/K)$. For the $M = 1$ term, we see that when the dispersion modulation is the dominant effect (i.e., when the approximate form of (141) applies), the effective nonlinear coefficient goes as $J_1(\Delta\tilde{k}/K) = J_1(\Delta\tilde{k}'/\Delta k')$, and thus for small modulation depth, is reduced by a factor of $(\Delta\tilde{k}'/2\Delta k')$ compared to homogeneous phase matching. Note that this is a factor $4/\pi$ smaller than the GAPM result of (131), which corresponds to the difference between the amplitude of the fundamental Fourier component of a unit amplitude square wave $(2/\pi)$ and a unit amplitude sine wave $(1/2)$.

If the grating is not sinusoidal, one can of course repeat this analysis for the various Fourier components of the grating function. The $4/\pi$ factor relating the GAPM result to (141) is easily recovered in this fashion. When the depth of the phase-modulation is small, the method is straightforward. However, when the modulation depth is large and the grating function is not sinusoidal, the result will contain sums of the sideband amplitudes resulting from several of the Fourier components of the grating, and algebraically complicated expressions are obtained.

VI. Summary

This paper has examined the theory of quasi-phase-matched SHG, and in particular, various departures from ideal QPM. The tuning properties of periodic structures were investigated, and phase-matching bandwidths due to the variations in temperature, wavelength, and propagation angle were obtained. The effects of a number of structural defects on the QPM conversion efficiency and tuning curves were then calculated. These results are of use both to estimate tolerances for device fabrication and as diagnostic tools for analyzing experimental measurements. Finally, a method of designing devices with tailored phase-matching curves was described.

Appendix I
Angle Tuning of Quasi-Phase-Matched SHG in Anisotropic Media

The analysis of angle tuning and bandwidths for SHG presented in Section II-C is valid only in isotropic media. While simple results are obtained illustrating effects due specifically to QPM, the analysis is not directly applicable to many experimentally important systems, e.g., interactions between extraordinary waves in periodically poled lithium niobate. In this appendix we extend the results of Section II-C to the more complicated case of anisotropic media.

The point of departure is again (37) and (38) relating the x and z components of the fundamental, second harmonic, and grating k vectors. For anisotropic media, the analysis is complicated by the angle dependence of the magnitude of k_1 and k_2, given by

$$k_1 = (\omega/c)n_1(\nu)$$
$$k_2 = (2\omega/c)n_2(\nu + \psi) \tag{A1.1}$$

where the variation of the indices of refraction depends on the orientation of the principal axes of the dielectric tensor and the magnitude of the birefringence. For notational simplicity, the symbol n_1 or n_2 with no argument is assumed to be evaluated at the angle given in (A1.1). With (37), (38), and (A1.1), and Fig. 2, we find that $d\Delta k/d\nu$ is given by

$$\frac{\partial \Delta k}{\partial \nu} = 2k_1 \cos(\nu)\left[1 + \frac{n_1'}{n_1}\tan(\nu)\right] \cdot \left\{-\tan(\nu+\psi)\frac{1 - \frac{n_2'}{n_2}\cot(\nu+\psi)}{1 + \frac{n_2'}{n_2}\tan(\nu+\psi)} + \tan(\nu)\frac{1 - \frac{n_1'}{n_1}\cot(\nu)}{1 + \frac{n_1'}{n_1}\tan(\nu)}\right\} \tag{A1.2}$$

where the prime indicates differentiation with respect to argument. (A1.2) can be shown to agree with (39) for isotropic media if we set $n_1' = n_2' = 0$. To first order in the derivatives of the indices of refraction (and hence to first order in the birefringence), (A1.2) can be written as

$$\frac{\partial \Delta k}{\partial \nu} = 2k_1 \cos(\nu)\left[1 + \frac{n_1'}{n_1}\tan(\nu)\right] \cdot \left\{[\tan(\nu) - \tan(\nu+\psi)] + \left[\frac{n_2'}{n_2}\sec^2(\nu+\psi) - \frac{n_1'}{n_1}\sec^2(\nu)\right]\right\}. \tag{A1.3}$$

Further analysis for arbitrary orientation of the principal axes is tedious. In the remainder of this appendix we assume that a principal axis of the dielectric tensor lies normal to the boundary and in the plane of incidence. We may then write the indices of refraction in the form

$$n_1(\nu) = n_1(0) + B_1 \sin^2(\nu)$$
$$n_2(\nu+\psi) = n_2(0) + B_2 \sin^2(\nu+\psi) \tag{A1.4}$$

where B_1 and B_2 are the birefringences at the fundamental and the second harmonic frequencies, and the form given, simpler than the exact result, is correct to first order in the birefringence. With (A1.4) in (A1.3), we obtain, to first order in B,

$$\frac{\partial \Delta k}{\partial \nu} = -2k_1\left\{\frac{\sin(\psi)}{\cos(\nu+\psi)}\left[1 + \left(\frac{2B_1}{n_1} - \frac{2B_2}{n_2}\right) - \frac{2B_1}{n_1}\cos^2(\nu)\right] + \left(\frac{2B_1}{n_1} - \frac{2B_2}{n_2}\right)\sin(\nu)\right\}. \tag{A1.5}$$

Note that for $B_1 = B_2 = 0$, (A1.5) agrees with (39) for isotropic media. According to (25), calculation of the angular acceptance bandwidth requires evaluation of the derivative in (A1.5) at the phase-matched angle $\nu = \nu_{PM}$, i.e., at the angle where $\Delta k = 0$. From (37) and (38) with $\Delta k = 0$ we find

$$\frac{\sin(\psi)}{\cos(\nu+\psi)} = \frac{(K/k_2)\sin(\kappa - \nu)}{(n_1/n_2)\cos(\nu) + (K/k_2)\cos(\kappa)}. \tag{A1.6}$$

With (A1.6) in (A1.5) we find

$$\left.\frac{\partial \Delta k}{\partial \nu}\right|_{\nu=\nu_{PM}} = -\left[\frac{K\sin(\kappa-\nu)}{\cos(\nu) + (K/2k_1)\cos(\kappa)}\right] \cdot \left[1 + 2\left(\frac{B_1}{n_1} - \frac{B_2}{n_2}\right) - \frac{2B_1}{n_1}\cos^2(\nu)\right] + 4k_1\left(\frac{B_2}{n_2} - \frac{B_1}{n_1}\right)\sin(\nu). \tag{A1.7}$$

The first term in (A1.7) consists of two factors, the first being the same as is obtained for QPM in isotropic media and the second a function of the birefringence that approaches unity for small birefringence. The second term

is the same as is obtained for conventional angle tuned SHG. We see that the contributions of the grating and the birefringence to the tuning rate are essentially additive, with a change in scale for the QPM term that is small if the birefringence is small. As for the isotropic case [(40)], the angular acceptance bandwidth can be obtained by inserting (A1.7) into (25), but the result of this simple substitution is not reproduced here.

Note that it is again possible to find a noncritical phase-matching angle for which $\partial\Delta k/\partial\nu = 0$. From (A1.7) it can be seen that noncritical phase-matching results from equal and opposite tuning rates from the birefringence and the grating. If the grating vector $\boldsymbol{K}$ is normal to the surface ($\kappa = 0$), it is clear that noncritical phase-matching can be achieved only if $\nu = 0$. To obtain the angular capacitance in this case, we must, according to (24), obtain the second derivative $\partial^2\Delta k/\partial\nu^2$. With (A1.7) we find

$$\left.\frac{\partial^2\Delta k}{\partial\nu^2}\right|_{\nu=0} = \frac{n_1}{n_2}\left[\Delta k' + 4k_1\left(\frac{B_2}{n_2} - \frac{n_2}{n_1}\frac{B_1}{n_1}\right)\right] \quad \text{(A1.8)}$$

which again takes the form of a sum of two terms, one that is the same as for QPM in an isotropic medium, and one that is the same as for conventional phase matching. With (A1.8) and (25) we find the tolerance for noncritical QPM in a birefringent medium,

$$\delta\nu = 2\sqrt{\left(1.772\,\frac{n_2}{n_1}\frac{l_c}{L}\left[1 + \frac{4k_1}{\Delta k'}\left(\frac{B_2}{n_2} - \frac{n_2}{n_1}\frac{B_1}{n_1}\right)\right]\right)^{-1}} \quad \text{(A1.9)}$$

Appendix II
Optimized Conversion Efficiency in Nonideal Structures

In an ideal quasi-phase-matched device, the peak conversion efficiency occurs at the nominal design wavelength, at which the k-vector mismatch obeys $\Delta k' = \Delta k_0'$. If the structure is nonideal, the conversion efficiency at the design wavelength is reduced by an amount that depends on the nature of the errors, and that can be calculated according to (13) or (48). In many cases, the k-vector mismatch can be offset a constant amount from the design point through temperature, angle, or wavelength tuning. It is interesting to ask at which value of the detuning the conversion efficiency of the nonideal structure is maximized. Assume that there are sufficiently many domains that the continuous approximation, (13), is valid. We may then write the normalized conversion efficiency as

$$\hat{\eta} = \|e^{i\Phi(z)}\|\,\|e^{-i\Phi(z)}\| \quad \text{(A2.1)}$$

where according to (7) and (11) the accumulated phase error is given by

$$\Phi(z) = \Phi_0(z) + \delta\Delta k z \quad \text{(A2.2)}$$

where $\Phi_0(z)$ is the phase error at the design wavelength, $\delta\Delta k$ is the offset added to maximize the efficiency, and

$$\|f(z)\| = \frac{1}{L}\int_0^L f(z)\,dz. \quad \text{(A2.3)}$$

If $\Phi_0(z)$ is small, we can expand (A2.1) to second order in $\Phi_0(z)$ to obtain

$$\hat{\eta} \approx 1 - [\|\Phi(z)^2\| - \|\Phi(z)\|^2]. \quad \text{(A2.4)}$$

with (A2.2) for $\Phi(z)$, (A2.4) becomes

$$\hat{\eta} \approx 1 - [\|\Phi_0^2\| - \|\Phi_0\|^2 + 2\delta\Delta k\|(z - L/2)\Phi_0\| + (L^2/12)\delta\Delta k^2]. \quad \text{(A2.5)}$$

Taking the derivative of (A2.5) with respect to $\delta\Delta k$, and setting the result equal to zero, we obtain the optimum offset,

$$\delta\Delta k_{\text{opt}} = -(12/L^2)\|(z - L/2)\Phi_0\|. \quad \text{(A2.6)}$$

Substituting this result into (A2.4), we obtain the optimized efficiency,

$$\hat{\eta}_{\text{opt}} \approx 1 - [\|\Phi_0^2\| - \|\Phi_0\|^2 - (12/L^2) \cdot \|(z - L/2)\Phi_0\|^2]. \quad \text{(A2.7)}$$

Equations (A2.6) and (A2.7), derived from expansions of (A2.1) correct to second order in the phase error, are generally applicable for small magnitude errors of arbitrary z dependence, and hence are useful for setting fabrication tolerances. If results are required for devices with errors sufficiently large that the efficiency is badly degraded, one can return to (A2.1) and analyze the efficiency for a specific type of error without making the series expansion used here, but little of a general nature can be said in this case.

Appendix III
Backward Propagating Interactions

If sufficiently short domains can be created, it is possible to quasi-phase-match interactions involving counterpropagating beams. Of special interest is backward parametric amplification, [47] which can lead to mirrorless parametric oscillation with counterpropagating signal and idler beams. Such devices have not been demonstrated due to the impractically large birefringence necessary for conventional phase matching in this configuration, but appear to be within reach of current QPM technology. Detailed discussion of parametric amplification is beyond the scope of this paper, but it is interesting to briefly investigate backward propagating SHG to illuminate basic features of such interactions.

The analysis given in Section II-C for angle tuning of QPM SHG is applicable to backward QPM (BQPM) simply by allowing θ to approach π. Equation (32) applies as written, and we find that the necessary period for BQPM is $\Lambda = m\lambda/2(n_1 + n_2)$. For $\lambda = 2\ \mu$m and $n_1 = n_2 = 2$, we find $\Lambda = m/4\ \mu$m, a difficult but not impossible target. Note that this is not the condition for QPM a degen-

erate backward optical parametric oscillator (BOPO), in which the signal and idler counterpropagate, and thus $\Lambda = m\lambda/2n_2$. The necessary grating period increases by a factor of two, becoming $\Lambda = m/2\ \mu$m for a 2 μm pumped BOPO operating at degeneracy.

For BQPM, certain of the tuning behaviors are quite different from those for collinear interactions. For example, the wavelength tuning bandwidth, corresponding to (30) becomes

$$\delta\lambda = \frac{0.4429\lambda}{L}\left|\frac{n_2 + n_1}{\lambda} + \frac{\partial n_1}{\partial\lambda} + \frac{1}{2}\frac{\partial n_2}{\partial\lambda}\right|^{-1}. \quad \text{(A3.1)}$$

Note that the sum, rather than the difference, of the indices, appears in the tuning rate, yielding a bandwidth of 0.4 nm in a 1 mm long device for the above example. As mentioned above, the angle tuning analysis can be applied as given in Section II-C, but the approximate forms that rely on the assumption $K << 2k_1$ of course are no longer valid. Finally, we note that the temperature acceptance bandwidth is also considerably narrowed, with (44) replaced by

$$\delta T = \frac{0.4429\lambda}{L}\left|\frac{\partial(n_1 + n_2)}{\partial T} + \alpha(n_1 + n_2)\right|^{-1}. \quad \text{(A3.2)}$$

The effect of thermal expansion is particularly large in this geometry, increased by a factor $(n_1 + n_2)/(n_1 - n_2)$ compared to the collinear case.

Note Added in Proof: Related work has recently been published by S. Helmfrid and G. Arvidsson, "Influence of randomly varying domain lengths and nonuniform effective index on second-harmonic generation in quasi-phase-matching waveguides," *J. Opt. Soc. Amer. B.*, vol. 8, pp. 797-804, 1991.

Acknowledgment

We would like to thank E. Lim for helpful discussions.

References

[1] J. A. Armstrong, N. Bloembergen, J. Ducuing, and P. S. Pershan, "Interactions between light waves in a nonlinear dielectric," *Phys. Rev.*, vol. 127, pp. 1918-1939, 1962.

[2] P. A. Franken and J. F. Ward, "Optical harmonics and nonlinear phenomena," *Rev. Mod. Phys.*, vol. 35, pp. 23-39, 1963.

[3] R. C. Miller, "Optical harmonic generation in single crystal $BaTiO_3$," *Phys. Rev.*, vol. 134, pp. A1313-A1319, 1964.

[4] J. Muzart, F. Bellon, C. A. Arguello, and R. C. C. Leite, "Generation de second harmonique non colineaire et colineaire dans ZnS accord de phase ('phase matching') par la structure lamellaire du cristal," *Opt. Commun.*, vol. 6, pp. 329-332, 1972.

[5] C. F. Dewey, Jr. and L. O. Hocker, "Enhanced nonlinear optical effects in rotationally twinned crystal," *Appl. Phys. Lett.*, vol. 26, pp. 442-444, 1975.

[6] L. O. Hocker and C. F. Dewey, Jr., "Enhancement of second-harmonic generation in zinc selenide by crystal defects," *Appl. Phys. Lett.*, vol. 28, pp. 267-270, 1976.

[7] B. F. Levine, C. G. Bethea, and R. A. Logan, "Phase-matched second harmonic generation in a liquid-filled waveguide," *Appl. Phys. Lett.*, vol. 26, pp. 375-377, 1975.

[8] M. S. Piltch, C. D. Cantrell, and R. C. Sze, "Infrared second-harmonic generation in nonbirefringent cadmium telluride," *J. Appl. Phys.*, vol. 47, pp. 3514-3517, 1976 (5 plates, $m = 5$).

[9] A. Szilagyi, A. Hordvik, and H. Schlossberg, "A quasi-phase-matching technique for efficient optical mixing and frequency doubling," *J. Appl. Phys.*, vol. 47, pp. 2025-2032, 1976 (2-5 plates, $m = 3$).

[10] D. E. Thompson, J. D. McMullen, and D. B. Anderson, "Second-harmonic generation in GaAs 'stack of plates' using high-power CO_2 laser radiation," *Appl. Phys. Lett.*, vol. 29, pp. 113-115, 1976 (1-12 plates, $m = 1$).

[11] M. Okada, K. Takizawa, and S. Ieiri, "Second harmonic generation by periodic laminar structure of nonlinear optical crystal," *Opt. Commun.*, vol. 18, pp. 331-334, 1976 (up to 24 quartz laminae, and 6 $LiNbO_3$ laminae, all with large m).

[12] Y. H. Xue, N. B. Ming, J. S. Zhu, and D. Feng, "The second harmonic generation in $LiNbO_3$ crystals with period laminar ferroelectric domains," *Chinese Phys.*, vol. 4, pp. 554-564, 1984.

[13] A. Feisst and P. Koidl, "Current induced periodic ferroelectric domain structures in $LiNbO_3$ applied for efficient nonlinear optical frequency mixing," *Appl. Phys. Lett.*, vol. 47, pp. 1125-1127, 1985.

[14] W. S. Wang, Q. Zhou, Z. H. Geng, and D. Feng, "Study of $LiTaO_3$ crystals grown with a modulated structure: I. Second harmonic generation in $LiTaO_3$ crystals with periodic laminar ferroelectric domains," *J. Cryst. Growth*, vol. 79, pp. 706-709, 1986.

[15] G. A. Magel, M. M. Fejer, and R. L. Byer, "Quasi-phase-matched second harmonic generation of blue light in periodically poled $LiNbO_3$," *Appl. Phys. Lett.*, vol. 56, pp. 108-110, 1990.

[16] M. C. Farries, P. St. J. Russell, M. E. Fermann, and D. N. Payne, "Second-harmonic generation in an optical fiber by self-written $\chi^{(2)}$ grating," *Electron. Lett.*, vol. 23, pp. 322-324, 1987.

[17] R. H. Stolen and H. W. K. Tom, "Self-organized phase-matched harmonic generation in optical fibers," *Opt. Lett.*, vol. 12, pp. 585-587, 1987.

[18] R. Kashyap, "Phase-matched period electric-field-induced second-harmonic generation in optical fibers," *J. Opt. Soc. Amer. B*, vol. 6, pp. 313-328, 1989.

[19] E. J. Lim, M. M. Fejer, and R. L. Byer, "Second-harmonic generation of green light in periodically poled planar lithium niobate waveguide," *Electron. Lett.*, vol. 25, pp. 174-175, 1989.

[20] J. Webjörn, F. Laurell, and G. Arvidsson, "Fabrication of periodically domain-inverted channel waveguides in lithium niobate for second harmonic generation," *J. Lightwave Technol.*, vol. 7, pp. 1597-1600, 1989.

[21] K. Nakamura and H. Shimizu, "Poling of ferroelectric crystals by using interdigital electrodes and its application to bulk-wave transducers," *1983 IEEE Ultrasonics Symp.*, pp. 527-530, 1983.

[22] C. J. van der Poel, J. D. Bierlein, J. B. Brown, and S. Colak, "Efficient type I blue second-harmonic generation in periodically segmented $KTiOPO_4$ waveguides," *Appl. Phys. Lett.*, vol. 57, pp. 2074-2076, 1990.

[23] G. Khanarian, R. A. Norwood, D. Haas, B. Feuer, and D. Karim, "Phase matched second harmonic generation in a polymer waveguide," *Appl. Phys. Lett.*, vol. 57, pp. 977-979, 1990.

[24] G. J. Edwards and M. Lawrence, "A temperature-dependent dispersion equation for congruently grown lithium niobate," *Optic. Quantum Electron.*, vol. 16, pp. 373-375, 1984.

[25] D. H. Jundt, M. M. Fejer, and R. L. Byer, "Optical properties of lithium-rich lithium niobate fabricated by vapor transport equilibration," *IEEE J. Quantum Electron.*, vol. 26, pp. 135-138, 1990.

[26] S. Somekh and A. Yariv, "Phase-matchable nonlinear optical interactions in periodic thin films," *Appl. Phys. Lett.*, vol. 21, pp. 140-141, 1972.

[27] C. L. Tang and P. B. Bey, "Phase matching in second-harmonic generation using artificial periodic structures," *IEEE J. Quantum Electron.*, vol. QE-9, pp. 9-17, 1973.

[28] B. Jaskorzynska, G. Arvidsson, and F. Laurell, "Periodic structures for phase-matching in second harmonic generation in titanium lithium niobate waveguides," *Proc. SPIE*, vol. 651, pp. 221-228, 1986.

[29] J. D. Bierlein, D. B. Laubacher, J. B. Brown, and C. J. van der Poel, "Balanced phase matching in segmented $KTiOPO_4$ waveguides," *Appl. Phys. Lett.*, vol. 56, pp. 1725-1727, 1990.

[30] J. Khurgin, S. Colak, R. Stoltzenberger, and R. N. Bhargava, "Mechanism for efficient blue second-harmonic generation in periodically segmented waveguides," *Appl. Phys. Lett.*, vol. 57, pp. 2540-2542, 1990.

[31] S. Somkeh and A. Yariv, "Phase matching by periodic modulation of the nonlinear optical properties," *Opt. Commun.*, vol. 6, pp. 301-304, 1972.

[32] Y. Yacoby, R. L. Aggarwal, and B. Lax, "Phase matching by periodic variation of nonlinear coefficients," *J. Appl. Phys.*, vol. 44, pp. 3180-3181, 1973.

[33] J. D. McMullen, "Optical parametric interactions in isotropic materials using a phase-corrected stack of nonlinear dielectric plates," *J. Appl. Phys.*, vol. 46, pp. 3076–3081, 1975.
[34] A. Yariv and P. Yeh, "Electromagnetic propagation in periodic stratified media. II. Birefringence, phase matching, and x-ray lasers," *J. Opt. Soc. Amer.*, vol. 67, pp. 438–448, 1977.
[35] R. C. Alferness, S. K. Korotky, and E. A. J. Marcatili, "Velocity-matching techniques for integrated optic traveling wave switch/modulators," *IEEE J. Quantum Electron.*, vol. QE-20, pp. 301–309, 1984.
[36] K. C. Rustagi, S. C. Mehendale, and S. Meenakshi, "Optical frequency conversion in quasi-phase-matched stacks of nonlinear crystals," *IEEE J. Quantum Electron.*, vol. QE-18, pp. 1029–1041, 1982.
[37] A. S. Chirkin and D. B. Yusupov, "Second harmonic generation by focused beams in layer media," *Sov. J. Quantum Electron.*, vol. 11, pp. 271–273, 1981.
[38] M. Nazarathy, D. W. Dolphi, and R. J. Jungerman, "Spread spectrum frequency response of coded phase reversal traveling wave modulators," *J. Lightwave Technol.*, vol. LT-5, pp. 1433–1443, 1987.
[39] G. D. Boyd, A. Ashkin, J. M. Dziedzic, and D. A. Kleinman, "Second-harmonic generation of light with double refraction," *Phys. Rev.*, vol. 137, pp. A1305–A1320, 1965.
[40] F. Zernike and J. E. Midwinter, *Applied Nonlinear Optics*. New York: Wiley, 1973, p. 138.
[41] N. P. Barnes and V. J. Corcoran, "Parametric generation processes: spectral bandwidth and accpetance angles," *Appl. Opt.*, vol. 15, pp. 696–699, 1976.
[42] M. Abramowitz and I. A. Stegun, *Handbook of Mathematical Functions*. Washington, DC: Nat. Bur. Stand., 1964, pp. 300–302.
[43] F. R. Nash, G. D. Brown, M. Sargent III, and P. M. Bridenbaugh, "Effect of optical inhomogeneities on phase matching in nonlinear crystals," *J. Appl. Phys.*, vol. 41, pp. 2564–2575, 1970.
[44] M. Nazarathy, D. W. Dolfi, and R. J. Jungerman, "Velocity-mismatch compensation in traveling-wave modulators using pseudorandom switched-electrode patterns," *J. Opt. Soc. Amer. A*, vol. 4, pp. 1071–1079, 1987.
[45] M. Nazarathy and D. W. Dolfi, "Spread-spectrum nonlinear nonlinear-optical interactions: quasi-phase matching with pseudorandom polarity reversals," *Opt. Lett.*, vol. 12, pp. 823–825, 1987.
[46] D. Ersame, D. A. Humphreys, A. G. Roddie, and M. G. F. Wilson, "Design and performance of phase reversal traveling wave modulators," *J. Lightwave Technol.*, vol. 6, pp. 933–936, 1988.
[47] S. E. Harris, "Proposed backward wave oscillation in the infrared," *Appl. Phys. Lett.*, vol. 9, pp. 114–115, 1966.

Martin M. Fejer, photograph and biography not available at the time of publication.

G. A. Magel, photograph and biography not available at the time of publication.

Dieter H. Jundt, photograph and biography not available at the time of publication.

Robert L. Byer (M'75–SM'83–F'87), for a photograph and biography, see p. 1117 of the April 1992 issue of this JOURNAL.